AMMRC CTR 77-12

[illegible] OF THE FATIGUE BEHAVIOR OF [illegible] REINFORCED COMPOSITES

March 1977

A. T. DiBenedetto

Mitsun Salee

University of Connecticut
Storrs, Connecticut 06268

CONTRACT NUMBER DAAG46-75-C-0064

[illegible]-Release; distribution unlimited.

[illegible] CENTER

Disclaimer

The findings contained in this report are not to be construed as an official Department of the Army position unless so designated by other authorized documents.

Citation of trade names in this report does not constitute an official endorsement or approval of the use of such items.

Destroy this report when no longer needed. Do not return it to the originator.

UNCLASSIFIED

SECURITY CLASSIFICATION OF THIS PAGE (When Data Entered)

REPORT DOCUMENTATION PAGE

READ INSTRUCTIONS BEFORE COMPLETING FORM

1. REPORT NUMBER: AMMRC CTR-77-12	2. GOVT ACCESSION NO.
3. RECIPIENT'S CATALOG NUMBER	
4. TITLE (and Subtitle): A Study of the Fatigue Behavior of Fiber Reinforced Composites.	5. TYPE OF REPORT & PERIOD COVERED: Final Report 3/1/75 to 6/30/76
	6. PERFORMING ORG. REPORT NUMBER
7. AUTHOR(s): A. T. DiBenedetto, Gideon Salee	8. CONTRACT OR GRANT NUMBER(s): DAAG46-75-C-0064
9. PERFORMING ORGANIZATION NAME AND ADDRESS: University of Connecticut, Storrs, Connecticut 06268	10. PROGRAM ELEMENT, PROJECT, TASK AREA & WORK UNIT NUMBERS: D/A Project: 1T162105AH84; AMCMS Code: 612105H80411; Agency Accession: DA OF 4742
11. CONTROLLING OFFICE NAME AND ADDRESS: Army Materials and Mechanics Research Center, Watertown, Massachusetts 02172	12. REPORT DATE: March 1977; 13. NUMBER OF PAGES: 103 (2) 111 pp.
14. MONITORING AGENCY NAME & ADDRESS (if different from Controlling Office)	15. SECURITY CLASS. (of this report): Unclassified
	15a. DECLASSIFICATION/DOWNGRADING SCHEDULE

16. DISTRIBUTION STATEMENT (of this Report)

Approved for public release; distribution unlimited.

17. DISTRIBUTION STATEMENT (of the abstract entered in Block 20, if different from Report)

18. SUPPLEMENTARY NOTES

19. KEY WORDS (Continue on reverse side if necessary and identify by block number)

Fatigue (materials)
Fiber composites
Graphite fibers
Polyaramid fibers

20. ABSTRACT (Continue on reverse side if necessary and identify by block number)

The fatigue failure of graphite fiber reinforced nylon is influenced by both the technique of fabrication of the composite and environmental conditions. Compression molded materials exhibited an isothermal brittle fatigue failure through initiation and propagation of cracks. Injection molded materials were non-linear, exhibiting ductile flow prior to ultimate failure. It is postulated that localized flow at a crack tip caused thermal melting, leading to a thermally induced fatigue failure. This study indicated (cont.)

over

DD FORM 1 JAN 73 1473 EDITION OF 1 NOV 65 IS OBSOLETE

UNCLASSIFIED

057 094900 R.L.H.

that processing characteristics such as fiber breakage, overlap and orientation strongly influence the fatigue endurance of the products.

Both fatigue life and tensile strength can be characterized by extreme value statistics and for a specific population there exists a unique relation between the cumulative distribution of tensile strengths and the cumulative distribution of fatigue lifetimes. It was found that for subpopulations derived from the same main population, an applied stress-breaking time superposition procedure (i.e. σ_{max} - log t_B) can be applied, with the shift factor being $\sigma_{max}/\langle\sigma\rangle$ dependent. Using the master curve, one can generate fatigue life distributions for different values of $\sigma_{max}/\langle\sigma\rangle$ within a reasonable degree of accuracy. The environmental shift seems to be totally expressed by the effect of the environment on the breaking strength distribution.

Damage propagation rate measurements indicate that under a constant set of upper and lower stress limits the rate of damage is constant. The rate of propagation was found to correlate best with a combination of the initial K_{max} and ΔK through the form

$$\dot{a} = f\left[K_{max}\left(1 - \frac{K_{min}}{K_{max}}\right)^{\alpha}\right]$$

Fatigue life prediction through the use of breaking strength distribution and damage propagation laws was tried. The model proposed was able to generate a reasonable distribution curve at a single set of experimental conditions. The damage propagation rate law had to be empirically modified however, in order to predict the distribution under different sets of experimental conditions.

Addition of polyaramid fibers to the graphite composites reduced the sensitivity of crack propagation to both the stress amplitude and the maximum stress. Hybrid composites were stronger and tougher than a graphite reinforced composite with an equivalent amount of fiber reinforcement.

ABSTRACT

The fatigue failure of graphite fiber reinforced nylon is influenced by both the technique of fabrication of the composite and environmental conditions. Compression molded materials exhibited an isothermal brittle fatigue failure through initiation and propagation of cracks. Injection molded materials were non-linear, exhibiting ductile flow prior to ultimate failure. It is postulated that localized flow at a crack tip caused thermal melting, leading to a thermally induced fatigue failure. This study indicated that processing characteristics such as fiber breakage, overlap and orientation strongly influence the fatigue endurance of the products.

Both fatigue life and tensile strength can be characterized by extreme value statistics and for a specific population there exists a unique relation between the cumulative distribution of tensile strengths and the cumulative distribution of fatigue lifetimes. It was found that for subpopulations derived from the same main population, an applied stress-breaking time superposition procedure (i.e. σ_{max} - log t_B) can be applied, with the shift factor being $\sigma_{max}/\langle\sigma\rangle$dependent. Using the master curve, one can generate fatigue life distributions for different values of $\sigma_{max}/\langle\sigma\rangle$ within a reasonable degree of accuracy. The environmental shift seems to be totally expressed by the effect of the environment on the breaking strength distribution.

Damage propagation rate measurements indicate that under a constant set of upper and lower stress limits the rate of damage is constant. The rate of propagation was found to correlate best with a combination of the initial K_{max} and ΔK through the form

$$\dot{a} = f\left[K_{max}\left(1 - \frac{K_{min}}{K_{max}}\right)^{\alpha}\right]$$

Fatigue life prediction through the use of breaking strength distribution and damage propagation laws was tried. The model proposed was able to generate

a reasonable distribution curve at a single set of experimental conditions. The damage propagation rate law had to be empirically modified, however, in order to predict the distribution under different sets of experimental conditions.

Addition of polyaramid fibers to the graphite composites reduced the sensitivity of crack propagation to both the stress amplitude and the maximum stress. Hybrid composites were stronger and tougher than a graphite reinforced composite with an equivalent amount of fiber reinforcement.

FOREWORD

There has been a growing use of short fiber reinforced polymeric solids in engineering components subject to fatigue failure, necessitating a more quantitative representation of the reliability of such structures. The objective of this research is to develop for fiber reinforced composites a framework for interrelating the statistical variability of the fracture process with the mechanical and environmental history of the structure.

The work described in this report was performed at the Institute of Materials Science, University of Connecticut, under Contract No. DAAG-46-75-C-0064. The research was sponsored by the Army Materials and Mechanics Research Center, Watertown, Massachusetts, with Dr. Margaret Roylance as Technical Supervisor.

TABLE OF CONTENTS

LIST OF FIGURES

List of Figures
(cont.)

LIST OF TABLES

I. INTRODUCTION

The reliability of fiber reinforced materials in engineering components subject to fatigue failure is of growing interest as these materials become more widely used. It is established that progressive fatigue damage, slowly building up to some critical value, is the principal mechanism of failure in fiber reinforced plastics (1-3). The fatigue process develops in three stages: nucleation of submicroscopic flaws, slow growth of flaws under repeated load and finally rapid propagation of cracks to catastrophic failure. Failure can occur by either thermal melting (through viscoelastic energy dissipation) or brittle failure (4). In this study we will examine brittle fatigue failure only.

Fiber reinforced plastics possess a distribution of submicroscopic and microscopic flaws whose character is determined primarily by the fabrication and handling history of the material. Upon application of a loading cycle, fatigue cracks nucleate and, from this instant, the fatigue life is controlled by their rate of growth. Although it is likely that initiation processes are important in unnotched polymer materials, there is little doubt that the multitude of fiber ends and debonded interfaces in fiber reinforced composites supply many sites for crack initiation during the very early application of stress (5,6).

In homogeneous solids the critical variable for characterizing the rate of crack growth is the stress intensity factor, K (7). For a unidirectionally stressed elastic body containing a crack of length (2a), the stress intensity factor may be written as:

$$K = Y \sigma(\pi(a + r_y))^{1/2} \qquad (1)$$

where Y is a geometrical parameter which depends on the specimen configuration (8), σ is the applied stress, (a) is the crack half-length

and r_y is the "plastic zone" size. The plastic zone around the tip of a crack in a polymeric material is the yielded or crazed material around the imbedded defect whose dimensions depend on the crack size and material properties. Dugdale (9) has shown that at stresses well below the yield point, $r_y = \frac{\pi}{8}(K^2/\sigma_y^2)$, where σ_y is the yield stress.

In viscoelastic polymers, a crazed zone develops around a crack tip with time. The crazed zone can grow at constant crack size until, at a critical time, the crack grows through the crazes. A number of theories for delayed crack growth in viscoelastic solids have been presented (10-14) which express both the rate of crazing and delayed crack growth as a function of stress intensity factor and time. A recent study of craze and crack growth in polycarbonate (14) indicates that both processes can be characterized by the same time dependent function.

Whether a stress intensity factor (developed for homogeneous solids) can be used to correlate crack growth in a heterogeneous, viscoelastic, fiber reinforced composite is certainly open to question. The stress field is complicated by the presence of multiple phases and the specification of a fracture criterion is complicated by factors such as fiber bridging at the crack tip. The use of a single value of critical stress intensity factor to mark the onset of catastrophic failure requires one to look upon the heterogeneous body as quasihomogeneous with respect to the fracture process. Available literature suggests that the breaking stress of isotropic short fiber reinforced materials is inversely proportional to the square root of crack size as expected by equation (1) (15-17) and that an "effective" stress intensity factor might be a useful material parameter.

In the first part of this study, a stochastic model relating the cumulative distribution of fatigue lifetimes directly to the cumulative

distribution of breaking stress is developed which by-passes the need of defining a stress intensity factor or measuring critical flaw size. In the second part of the study the rate of crack growth from a manufactured notch is measured as a function of "effective" stress intensity factor and the resulting equations are used to calculate directly the fatigue lifetime.

II. STATISTICS OF BRITTLE FRACTURE

Brittle fracture generally originates in highly localized regions where stress is concentrated at submicroscopic flaws. Fracture of a specimen at a given level of stress depends on the statistical expectations of encountering a critical (or weakest) flaw having the specified strength. If flaws are distributed at random throughout a population, the distribution of strengths is statistically related to the distribution of largest flaws appearing throughout the population. This model is identical to the generalized asymptotic theory of extreme values (18). For samples consisting of n elemental volumes having a probability density function of elemental strength $f(\sigma)$ (i.e. $f(\sigma)d\sigma$ = fraction of elements having a strength between σ and $(\sigma + d\sigma)$) and cumulative distribution of elemental strengths $F(\sigma) = \int_0^\sigma f(\sigma)d\sigma$, the distribution of smallest values of σ (i.e. the fraction of specimens with a strength between σ and $(\sigma + d\sigma)$) is given by:

$$g_n(\sigma) = nf(\sigma)(1 - F(\sigma))^{n-1} \tag{2}$$

and the cumulative distribution of sample strengths is given by:

$$G_n(\sigma) = \int_0^\sigma g(\sigma)d\sigma = 1 - (1 - F(\sigma))^n \tag{3}$$

This is the probability of encountering a specimen with a strength equal to or less than σ. For the case of fracture, the elemental probability

function $f(\sigma)$ is unknown since the random variable σ cannot be measured directly except for the extreme value itself (i.e. the fracture stress of the material).

A model for the function $f(\sigma)$ has been developed by Weibull based on experimental data on the cumulative distribution of sample strengths $G(\sigma)$ (19). A two parameter version of the Weibull function is:

$$f(\sigma) = \frac{\alpha}{\sigma_0} \left(\frac{\sigma}{\sigma_0}\right)^{\alpha-1} \exp - \left(\frac{\sigma}{\sigma_0}\right)^{\alpha} \tag{4}$$

which results in a cumulative distribution of sample strengths given by:

$$1 - P(\sigma) = G(\sigma) = 1 - \exp - n\left(\frac{\sigma}{\sigma_0}\right)^{\alpha} \tag{5}$$

where σ_0 and α are constants and n is the number of elemental volumes in the material. (For a population with specimens of fixed volume, n is constant and may be combined with the constant σ_0.). This type of equation is widely used to characterize the variability of strength in fiber reinforced composites (20-25).

The results of fatigue tests can also be characterized by the statistics of extreme values. The specimens that fail under a given stress amplitude at various numbers N of load cycles may be considered as forming a group of the weakest specimens out of a large population of samples. The distribution of N among this subpopulation may therefore be described by a Weibull function of the form (26):

$$1 - P(N)_S = G(N)_S = 1 - \exp - \left(\frac{N}{N_0}\right)^{\alpha_f} \tag{6}$$

where G(N) is the cumulative probability of encountering a specimen with a life of N cycles or less under a stress of amplitude S. The parameters N_0 and α_f are constants.

Equations 5 and 6 are only two of a variety of cumulative distribution functions that might be used to describe the strength and fatigue life

distributions of fiber reinforced materials. More complex forms must be used when factors such as a lower limiting strength, endurance limits, bimodal elemental probability distributions or induction times for crack nucleation must be considered. For the specific materials studied herein, however, the above mentioned equations appear to be adequate.

Regardless of the exact functional forms for the cumulative distribution equations, it is likely that if both breaking strengths and cycles to failure can be described as Poisson processes, one should be able to find a functional relationship between the two quantities at equiprobability points in the respective distributions, i.e.:

$$(N)_s = f(\sigma_b) \; @ \; P(N)_s = P(\sigma_b) \tag{7}$$

This idea will be used to develop a single "master-curve" of fatigue-life versus breaking strength for a given population of material. The master curve will then be used to estimate changes in fatigue lifetime caused by environmental degradation.

III. A MODEL FOR FATIGUE CRACK PROPAGATION

It is generally agreed that failure initiates from critical flaws in the material structure. Thus, if one knows the initial flaw size and the rate of flaw growth under a given loading history, one should be able to estimate the time-to-break. There have been a variety of crack propagation laws suggested in the literature (27,28). An appropriate function for crack propagation in fiber reinforced plastics incorporates the effects of a maximum stress intensity factor K_{max}, the amplitude of stress (in the case of fatigue), a lower threshold below which no crack propagation occurs (K_{th}) and an upper limiting value above which crack propagation is instantaneous (K_c) (29). A model was chosen that was a

combination of one used by Erdogan (30) for crack propagation in fatigue and by Kitagawa and Motomura for crack growth in viscoelastic solids (14):

$$\dot{a} = \beta \left[\frac{(ERD)^2}{-\ln \left(1 - \frac{(\frac{ERDC}{ERD})^2 - 1}{(\frac{ERDC}{ERDT})^2 - 1}\right)} \right]^{\alpha} \tag{8}$$

where $\dot{a}$ is the flaw grow rate, β is a rate constant dependent on temperature, frequency, environment etc., α is a constant and ERD is the variable defined by the following equation:

$$ERD = K_{max} (1 - R)^{\gamma} \tag{9}$$

The variable K_{max} is the stress intensity factor at the maximum stress in the test, R is the ratio of maximum to minimum stress (or stress intensity) during fatigue and γ is a constant. The lower threshold is characterized by $ERDT = K_{Th} (1-R)^{\gamma}$ and the upper threshold is given by $ERDC = K_C(1-R)^{\gamma}$.

Although it is felt that this is a realistic model for crack growth in the systems that have been studied, it is recognized that a five-parameter model is not required for adequate fitting of most experimental data that is presently available. An equation of the form (30):

$$\dot{a} = \beta[K_{max} (1-R)^{\gamma}]^{r} = \beta[K_{max}^{1-\gamma} \Delta K^{\gamma}]^{r} \tag{10}$$

although not containing an upper and a lower bound, fits most data quite satisfactorily (29).

Very little data on composites are available, but models similar to the above mentioned are used for correlation (31-35). In orthotropic laminates, resistance to crack propagation is a function of orientation

and there are a variety of energy dissipating mechanisms including fiber/matrix debonding to blunt crack propagation (36-38). Studies on randomly dispersed-short fiber reinforced materials (15,17) indicate that an equation of the form:

$$\dot{a} = \beta(\Delta K)^{\alpha}, \tag{11}$$

where ΔK is the amplitude of the stress and β and α are constants, is satisfactory for fitting the experimental data.

IV. FATIGUE LIFE PREDICTION

Several approaches to fatigue life predictions in composites have been tried (39-41). Broutman and Sahu (39) used a modified version of Miner's law to describe lifetime distributions for a population of E-glass reinforced epoxy. For a similar system, Agarwal and Dally (40) found that fatigue life could be correlated to a normalized stress $(\Delta\sigma)/\sigma_u$:

$$\frac{\Delta\sigma}{\sigma_u} = \alpha - \beta \log N \tag{12}$$

where $\Delta\sigma$ is stress amplitude σ_u is ultimate strength and N is cycles to break. Salee (29) and Hahn (24) have found unique relationships between breaking strength distributions and fatigue life distributions. A more general approach to fatigue life prediction has been introduced by Halpin et. al. (41). They use a Weibull distribution function and a power law growth model to obtain a cumulative distribution equation of the form:

$$P(\sigma_b(t)>\sigma) = \exp - \left[\left(\frac{\sigma_b(t)}{\hat{\sigma}}\right)^{2(r-1)} + \left(\frac{t}{\hat{t}}\right)\right]^{\alpha_f} \tag{13}$$

where r, $\hat{\sigma}$, $\hat{t}$ and α_f are constants and $\sigma_b(t)$ is residual strength at time t. Equation (13) can be used to calculate the cumulative strength distribution at a specified time $t = t_o$ or to calculate a cumulative distribution of breaking times, $P(t_B)$ at a specific residual strength $\sigma_b(t) = \sigma_{max}$.

V. FATIGUE BEHAVIOR OF SHORT GRAPHITE FIBER REINFORCED NYLON 66 COMPOSITES

Cumulative distribution functions for both tensile strength and time-to-break in fatigue were generated for several populations of graphite fiber reinforced nylon 66. In addition, crack propagation rate data were obtained. It will be shown that for a population of composite materials there is a unique relationship between tensile strength and fatigue life and that a-priori prediction of fatigue lifetime from crack propagation rate data is extremely difficult because of the high sensitivity of propagation rate to stress.

1. Experimental Procedures

Materials

The experimental work was performed on short graphite fiber-reinforced nylon 66 materials. The nylon 66 was a 60-80 mesh powder of DuPont's Zytel 101. The average modulii of compression molded specimens of the nylon were 1.8×10^5 psi and 7×10^4 psi at 55 and 100 percent relative humidity respectively. The graphite fibers were Hercules type AS, with 6 mm. average length, 8.4×10^{-3} mm. average diameter, 420,000 psi average strength, 32×10^6 psi average modulus of elasticity and 1.8 grams/cc (0.065 lb/in^3) density. Two batches of fibers, obtained one year apart, were used. The two batches were somewhat different in properties and will heretofore be referred to as fiber batch 1 and fiber batch 2. The compression molding fabrication technique has been reported previously (23).

The composite samples contained 10% by volume of fiber in a random-in-a-plane orientation. Standard 6.5 inch tensile bars were machined from 1/8 inch thick composite plates. Cantilever beams for use in the crack propagation experiments were 6 in. by 1/2 in. by 1/8 in. Precisely placed channels were cut in the center of each half-inch face parallel to the length forming a path for crack propagation. A sharp crack 1.0 in. in length was cut into one side of the beam between the loading points. In addition to the compression molded specimens prepared in the laboratory, a series of injection molded tensile bars containing 13.7 volume per cent fibers were obtained from LNP Corporation.

The test specimens were annealed for 24 hours in a silicone oil bath at 185°C. They were then conditioned for 24 hours in a boiling 48 per cent aqueous solution of potassium acetate. During this process the composite absorbs 2.8 per cent water which is equal to the equilibrium adsorption in air at 50 per cent relative humidity.

Mechanical Testing Procedure

Tensile stress-strain measurements were made on an Instron Model 1230 hydraulically actuated testing machine at a crosshead speed of 0.2 in. per minute and room temperature. The average cross-sectional area in the gauge length and the actual cross-section at the break were measured and the elastic modulus, breaking strength, proportional limit and elongation at break were determined.

Cumulative distribution curves for tensile fatigue at 10 cycles per second were also obtained. The maximum and minimum loads for the fatigue test were calculated and the machine set in the load control mode. In this mode the load limits are maintained regardless of the creep in the sample. In load control, the mean load and command are first set to zero. The function generator is set to give a sine wave at 10 Hertz and then the mean load is increased to the required amount. The command dials are increased until the maximum and minimum load limits are obtained. This process usually took of the order of 10 seconds or roughly 100 cycles. At this point the cycle counter is started and the test begins.

Flaw Propagation Rate Measurements

In the graphite fiber reinforced materials, opacity, crack bridging by broken fiber ends and irregularly shaped fracture surfaces made it impossible to follow the crack tip visually. The propagation rate was measured indirectly by measuring crack opening displacement. The pre-notched cantilever beams were precalibrated by machining cracks of a given size and measuring beam compliance and crack opening displacement as a function of load. An effective stress intensity factor was defined by the usual definition in terms of compliance of a double cantilever:

$$K^2 = \frac{3P^2}{Wb} \left[\frac{4(a + 0.6h)^2}{h^3} + \frac{1-\nu}{h} \right] \qquad (14)$$

where P is the applied force at the loading pins, W is the width of the notched section, b is beam width, h is the beam height, ν is Poisson's Ratio and a is the flaw length.

2. Experimental Results and Analysis of Data

Data are reported on four populations of graphite fiber reinforced nylons which will be given the following designations

TABLE 1. Experimental Populations

Designation	Treatment
1 A $\frac{1}{2}$ RH 55	Nylon 66, Fiber Batch 1, compression molded, annealed 1/2 hour, conditioned at 55 percent relative humidity
1 A 1 RH 100	Nylon 66, Fiber Batch 1, compression molded, annealed 1 hour, conditioned at 100 per cent relative humidity
2 A 24 R.H. 55	Nylon 66, Fiber Batch 2, compression molded, annealed 24 hours, conditioned at 55 per cent relative humidity
LNP	Commercially available graphite reinforced nylon 66, annealed 24 hours and conditioned at 55 per cent relative humidity

The tensile stress-strain curves were linear up to the breaking point except for 37 percent of the specimens in the 1 A 1 RH 100 population which showed some yielding at 9500 ± 300 psi. The initial moduli of elasticity are presented in Table 2:

TABLE 2. Moduli of Elasticity

Population	Modulus of Elasticity psi
1 A $\frac{1}{2}$ RH 55	950,000 ± 100,000
1 A 1 RH 100	795,000 ± 145,000
2 A 24 RH 55	1,079,000 ± 265,000
LNP	1,407,000 ± 231,000

The lower modulus in the 1 A 1 RH 100 specimens relative to that of the 1 A 1/2 RH 55 is caused by the lower modulus of water saturated nylon 66 (7×10^4 psi) compared to nylon 66 at 55 percent humidity (1.8×10^5 psi). The slightly higher modulus of the 2 A 24 RH 55 population is caused by a somewhat higher degree of crystallinity in the nylon annealed for 24 hours. The variability in all cases is associated primarily with compositional variations from piece to piece. A one percent variation in the fiber composition (reasonably expected with the layup procedure employed) can lead to a ± 120,000 psi variation in the modulus. The theoretical moduli, calculated using the Pagano-Tsai equation (42), are 1.29×10^6 psi and 1.01×10^6 psi for the populations conditioned at 55 percent RH and 100 percent R.H. respectively. Fiber efficiencies are thus of the order of 75 to 85 percent, indicating good stress transfer from matrix to fiber. The higher modulus of the LNP fibers is due to the higher fiber loading (13.7 per cent rather than 10 per cent).

The cumulative distributions of tensile strengths are shown in Figures 1 and 2. All populations conform to a simple Weibull function with coefficients of determination greater than 98 per cent. The Weibull parameters, the average breaking strengths and the coefficients of variation are summarized in Table 3.

TABLE 3 Weibull Parameters for Tensile Strength Distribution Function

Population	α	$\hat{\sigma}$ (psi)	$\langle\sigma\rangle$ psi	Coeff. of Var.
1A 1/2 RH 55	9.9	13,144	12,409	0.112
1 A 1 RH 100	11.7	11,446	10,985	0.078
2 A 24 RH 55	14.8	16,768	16,190	0.078
LNP	23.6	20,097	19,688	0.047

If we estimate that the theoretical strength of a random-in-a-plane reinforced composite is roughly equal to one-third of the value predicted by the rule-of-mixtures, the predicted average strength should be of the order of 16,000 to 17,000 psi (based on a fiber strength of 420,000 psi and a nylon strength of 8,300 psi at 55% RH and 6,300 psi at 100% RH). This leads to fiber utilization efficiencies of 70 to 90 per cent, which are in agreement with the values calculated from the modulus. The Weibull parameters for the 2 A 24 RH 55 population were higher than for the other compression molded populations. This group of specimens was prepared using a different batch of fibers. Although the two were supposedly identical, it appears that the fibers in the second batch are somewhat stronger and have less variation in their strength. (In retrospect it was recalled that the handleability of the two fiber batches was also somewhat different). The coefficient of variation for the LNP injection molded materials is much smaller, indicating a more reproducible process for preparing the specimens. The conditions for the cyclic fatigue tests are summarized in Table 4:

TABLE 4 Stress Amplitudes in Fatigue Experiments

Population	Conditions			
	σ_{max} psi	σ_{mean} psi	$R = (\sigma_{min}/\sigma_{max})$	$\sigma_{max}/\langle\sigma\rangle$
1 A 1 RH 100-1	9061	5458	0.20	0.83
1 A 1 RH 100-2	9279	5458	0.18	0.85
1 A 1 RH 100-3	9824	5458	0.11	0.90
1 A 1/2 RH 55	11250	6250	0.11	0.90
2 A 24 RH 55	13566	8172	0.20	0.83
LNP	13788	7873	0.14	0.70

Because the maximum stress in the tests were close to the average strengths of the populations, a fraction of the weaker specimens broke on the first half-cycle (represented by G(o) below). The 1 A 1 RH 100-1 population also possessed a considerable number of specimens surviving over 10^6 cycles (10^5 seconds), indicating that these composites have an endurance limit that is at a relatively high stress level. The Weibull function used to describe the data was modified to account for the above mentioned facts:

$$P(t_B) = (1-G(o)) \exp - (t_B - t_o/\hat{t})^{\alpha f} + P(\infty) \qquad (15)$$

The parameters, determined by a linear regression analysis, are given in Table 5, while plots of the data are shown in Figures 3 and 4.

TABLE 5 Weibull Parameters for Fatigue Life Distribution Function

Population	α_f	$\hat{t}$ (seconds)	G(o)	P(∞)	t_o seconds
1 A 1/2 RH 55	0.68	4661	0.103	0.000	0
1 A 1 RH 100-1	0.44	5852	0.148	0.148	0
1 A 1 RH 100-2	0.44	6576	0.000	0.000	0
1 A 1 RH 100-3	0.82	520	0.273	0.000	0
2 A 24 RH 55	0.59	6034	0.093	0.000	0
LNP	0.53	828	0.000	0.000	298

Coefficients of determination are greater than 95 per cent for all cases.

Crack propagation rate measurements were carried out on specimens from the three compression molded populations. The interaction between the stress intensity range, ΔK, and the absolute value of the maximum stress intensity, K_{max}, was determined by changing both values during the course of an experiment.

The most important characteristic of the flaw propagation is that the rate depends only on the initial value of the stress intensity parameter. At a fixed value of σ_{max} and R, the flaw propagation rate is constant for almost the whole life of the specimen. Only in the last few cycles of life does the flaw growth rate accelerate. Thus, the mechanism of failure is as follows: Stress concentration around the flaw tip causes the region around the tip to progressively decrease in strength. This zone grows linearly in time, but the actual crack tip does not move. When the material has been weakened enough, crack propagation occurs rapidly and failure ensues. If the load is increased prior to catastrophic failure, the crack opens and grows to a new "equilibrium" size and the damage then occurs at a faster constant rate. This is similar to the mechanism of craze growth in amorphous plastics under stress corrosion environments.

The Erdogan equation (Eqn. 10) provided a suitable function for correlation. By letting the exponent γ vary from 0.0 to 1.0, the relative influence of K_{max} and ΔK could be explored. By running a regression analysis, the values of γ and r giving the best fit of the data can be found. The results for the three populations are presented in Table 6. A typical plot of the experimental data is shown as Figure 5.

TABLE 6. Parameters for the Erdogan Eqn. (10).

Population	β (ȧ in cm/min)	γ	r	Coeff. of Det.	$\dot{a}\ \frac{cm}{min}$ @ R=0.2 & K_{max}=400 kg-cm$^{-3/2}$
1 A 1 RH 100	7.68×10^{-42}	0.6	15.0	0.69	1.24×10^{-3}
1 A 1 RH 55	4.36×10^{-47}	0.1	16.4	0.72	1.43×10^{-4}
2 A 24 RH 55	1.68×10^{-57}	0.4	19.4	0.83	8.98×10^{-8}

The last column of Table 6 indicates the crack propagation rates at K_{max} = 400 kg-cm$^{-3/2}$ and R=0.2, which are representative of the values used in the fatigue experiments. The 1 A 1RH 100 population is least resistant to crack propagation, while the 2 A 24 RH 55 population is most resistant. Although a linear plot on log-log coordinates appears reasonable (Figure 5), the coefficients of determination are rather low. A plot of the data on an expanded scale for the 1 A 1 RH 100 population is shown in Figure 6 and suggests the source of the low correlation. The data appear to indicate both a lower and upper threshold for crack propagation as suggested by equation (8), but the scatter of experimental results, associated with uncertainties in the measured values of both velocity and maximum stress intensity make it difficult to find a "better" model. A grid search technique was used to evaluate the parameters in equation (8). Results for two systems are presented in Table 7.

TABLE 7. Parameters for Equation (8).

	β	ERDC	ERDT			
	ȧ in cm/min	k g - cm$^{-3/2}$		γ	α	Coeff. of Det.
1 A 1/2 RH 55	0.93×10^{-8}	635	425	0.1	1.0	0.70
1 A 1 RH 100	4.95×10^{-12}	560	315	0.6	1.7	0.71
1 A 1 RH 100 (based on fatigue data)	1.42×10^{-16}	521	354	0.6	2.1	0.68

Coefficients of determination were of the same order as before, in spite of two additional parameters. (The third entry in Table 7 will be discussed later). When crack propagation rate is so highly sensitive to stress intensity factor, it will be very difficult to develop models with a greater degree of certainty than those presented above.

3. Fatigue Life Prediction: Correlation Between Tensile Strength and Fatigue Life

The cumulative distributions of both static tensile strength and fatigue lifetimes have been represented by Weibull functions. As suggested by equation 7, one should be able to find a functional relation between these two variables at equivalent points in their respective distributions. Using the data in Tables 3 to 6, one can generate the following master curve for all the data obtained on composites containing fibers of batch 1:

$$\log_{10} \sigma_b = 0.112 \left[\frac{\sigma_{max}}{\langle\sigma\rangle} (1-R)^{0.5}\right]^4 \log_{10} t_B + 3.915 \quad (16)$$

The result is plotted in Figure 7. The coefficient of determination for the straight line is 0.99. Thus, all the data for a given population of composites, made by the same fabrication process and using the same raw materials, can be reduced to a single master curve. The effects of stress and environment on the fatigue life can therefore be determined from the effects on the distribution of tensile strengths.

The relation for the composites prepared using fibers of batch 2 is:

$$\log_{10} \sigma_b = 0.101 \left[\frac{\sigma_{max}}{\langle\sigma\rangle} (1-R)^{0.5}\right]^4 \log_{10} t_B + 4.114 \quad (17)$$

The curve is nearly parallel to the former, but displaced to lower values on the time scale (Figure 7). The slopes of these plots are

associated with the dispersion of the cumulative distributions and are thus related to the distribution of flaws in the two populations. Since the distribution of flaws is probably controlled mainly by the fabrication process, the two populations should exhibit a parallel response. The "intercepts" are controlled by both the scale and dispersion of the distributions and are clearly different for the two fiber batches. In this case, the added fiber strength does not translate into a proportional increase in fatigue life.

4. Fatigue Life Prediction From Crack Propagation Data

The wearout model (41), equation 13, was tested as a tool for fatigue life prediction. The experimental data were used in a grid search technique and a linear regression procedure to determine the constants r, $\hat{t}$ and $(\sigma_{max}/\hat{\sigma})^{2(r-1)}$ of equation (13). The results are summarized in Table 8.

TABLE 8. Parameters for Wearout Model (Eqn. 13)

Population	r	$\hat{t}$(sec)	$(\sigma_{max}/\hat{\sigma})^{2(r-1)}$	Coeff. of Determination
1 A 1/2 RH 55	11.5	3116	-4100	0.96
1 A 1 RH 100-1	22.8	919	-0.10	0.98
1 A 1 RH 100-2	16.5	1060	0.16	0.96
1 A 1 RH 100-3	18.8	102	-0.99	0.98
2 A 24 RH 55	19.0	365	-0.12	0.98

Although the model fits the data very well, the quantity r is not independent of environmental conditions, as assumed, and the "best-fit" value of $(\sigma_{max}/\hat{\sigma})^{2(r-1)}$ is negative in many cases, which is not physically correct. It is quite possible that a three parameter optimization could

lead to other "best-fit" values, but it is felt that these problems render the model much less useful as a tool for fatigue life prediction for these materials.

A prediction of the breaking time in fatigue directly from the crack propagation rate equations was also attempted. The procedure is described below and illustrated in Figure 8.

Start with the distribution curve for 1 A 1/2 RH 55. Since σ_{max} is 11,250 psi, specimens with breaking strengths less than or equal to this value must have zero breaking time. Thus, from Table 7 and equation 8, ERD → 635 (i.e. $a \to \infty$) at the point on the distribution corresponding to σ_b = 11,250 psi (at $P(\sigma_b) = 0.8$). The value of the parameter (ERD), and thus the crack propagation rate $\dot{a}$, can be calculated at any other point on the distribution since $(ERD)_1/(ERD)_2 = \sigma_{b2}/\sigma_{b1}$. At $P(t_B) = P(\sigma_b) = 0.5$, for example, ERD = 563 and $\dot{a}$ = 0.012 cm/min. Using this point as a reference point, one may then calculate the relative crack propagation velocity at any other point on the distribution. Since the growth rates are constant for most of the life of the material, one may assume the relative breaking times are inversely proportional to the relative velocities (i.e. $\dot{a}_1/\dot{a}_2 = t_{B2}/t_{B1}$). The solid curve in Figure 8 has been generated in this fashion and follows the exprimental distribution very closely. In a similar manner, one may use this reference point and the crack propagation data for the other populations to generate theoretical distributions of fatigue life at other conditions. This was attempted using the "best-fit" values for the crack propagation rate (Table 7). The predicted distribution was too sharp (Eqn. 1 of Figure 8). The calculations were redone using a different set of values in the crack propagation equation (3rd line of Table 7 and Figure 6) with a high

degree of success. The solid lines in Figures 4 and 8 were generated in this manner.

Unfortunately, we cannot find any a-priori justification for using the latter set of parameters to describe the crack propagation data for the 1 A 1 RH 100 population, other than the fact that they are consistent with the breaking time results. Because of the high sensitivity of crack propagation to stress level and the inability to make more precise measurements of the damage rate, predictions of lifetime directly from the propagation rate data must be recognized as highly unreliable for this system.

5. Mechanism of Fatigue Failure

It was observed that damage propagation rates remained constant for a fixed level of upper and lower cyclic stresses and that as the stress levels were changed, the damage propagation rate also changed. This suggests that the propagation rate depends on the stress intensities operating at the tip of the initial crack and that the damaged region around the crack tip grows (or decreases in strength) in such a way that the effective magnitude of stress concentration at the crack tip does not change. A similar behavior was reported for environmental craze growth in PMMA (43).

Owen and Dukes (44) observed that in random chopped strand E-glass reinforced laminates the individual strands lying perpendicular to the stress direction were the first sites of damage. The damage took place in the form of debonding (i.e. separation between the fiber and the matrix) that intensified progressively, affecting fibers at smaller angles to the applied load until at some higher load (less than the ultimate load) resin cracks occurred in the resin rich zone of the material.

In the nylon-graphite composite, the early damage also occurs near fibers lying perpendicular to the stress direction. However, as can be seen in Figure 9, instead of fiber debonding (which may also occur to a small extent), good adhesion to the fibers causes the resin to draw in the direction of the stress. The high degree of elongation causes the fibers in this region to break randomly. Broken ends may provide nuclei for the concentric striations pictured in Figure 10. This process may be accompanied by cavitation of the resin about the fiber, which involves drawing of the resin in a direction radial to the fiber. Fibers which break prior to matrix failure have to be pulled out during the crack opening process. The length of fiber that has to be pulled out (i.e. half the critical fiber length lc/2) is estimated to be 0.12 to 0.17 mm. The breaking of fibers, the pull out of fibers bridging the damaged matrix and the drawing and cavitation of the resin about the fibers are the major energy dissipating processes occurring in the region around the crack tip. The damage zone around the crack tip grows linearly with time while the actual crack tip is stationary.

This is phenomenologically similar to the drawing and cavitation of polymer bridging the faces of a propagating craze. Once the damage zone reaches its critical dimensions, a fast crack propagates at a rate that does not allow further plastic deformation to occur.

6. Fatigue Mechanism: Comparison Between Injection Molded and Compression Molded Populations

One can see that the average strength of the injection molded specimens is higher than that of the compression molded materials and that the cumulative distribution for the injection molded materials is narrower than that of the compression molded population. The lower coefficient of variation shows the higher degree of reproducibility of the injection molding technique (Figure 2).

The cumulative distribution of breaking times for two populations tested under approximately the same conditions of stress are plotted in Figure 3. Although the upper limits of the stress amplitude applied to both populations are almost the same, the injection molded specimens were fatigued at only 70% of their average strength while the compression molded samples were fatigued at 83% of the average strength. In spite of this, the mean breaking time (measured at $P(t_B) = 0.5$) is 680 seconds for the injection molded compared to 2700 seconds for the compression molded materials. The compression molded specimens have an average fatigue life clearly superior to the injection molded specimens. On the other hand, the compression molded specimens show a much broader variation in fatigue life and, in fact, the lower 20% of the distribution lies below that of the injection molded materials. Thus, although the average properties are superior, one would have to expect a greater number of early failures in the compression molded populations. In this case, "reliability" is not related to "average lifetime".

Typical temperature measurements as a function of time are shown in Figure11. In all cases, the surface temperature of the injection molded specimens increased steadily with time until the specimen failed at a temperature in the range of 70-80°C. On the other hand, the temperature of the compression molded specimens reached a steady state of approximately 30-35°C after a few hundred seconds.

This suggests that the macroscopic ductility of the injection molded materials led to a viscous heating of the material and that the failure mechanism was at least partially influenced by the thermal effect. The induction time t_o = 298 sec. is most likely the minimum time required to heat the specimen to a critical temperature under the test conditions. The compression molded specimens, on the other hand, are linearly elastic to the point of failure and heating is due only to viscoelastic energy dissipation. The failure, in this case, is an isothermal, brittle fracture.

Scanning electron micrographs of fracture surfaces from the two populations are shown in Figures 12 and 13. The surfaces of injection molded specimens clearly show thermal melting and a subsequent dewetting of the fibers in the slow crack region. Photographs of the fast crack region confirm that the adhesion was initially present. The fracture surfaces of the compression molded materials, on the other hand, show good adhesion at all points. Examination of suspensions of recovered fibers from injection molded specimens indicates considerable damage and a wide distribution of fiber lengths (Figure 14). Fiber lengths vary between 0.01 and 1.0 mm with an average length being of the order of 0.1 to 0.3 mm. The average aspect ratio is thus about 18. The fibers also exhibit a longitudinal orientation. This was determined by dissolving away nylon at the surface of the material and examining the exposed fibers by dark field photography (Figure 15). This preferred orientation is undoubtedly contributing to the apparent high fiber efficiency. The compression molded specimens, on the other hand, show random orientation and no damage from processing.

VI. FATIGUE BEHAVIOR OF POLYARAMID/GRAPHITE FIBER REINFORCED NYLON 66 COMPOSITES

1. Fabrication of Composite Test Specimens

The experimental work was performed on four types of composite.

1. A 20 per cent by volume short graphite fiber reinforced Nylon 66.
2. A 20 per cent by volume short polyaramid fiber reinforced Nylon 66.
3. A 10 per cent short graphite/10 per cent polyaramid fiber reinforced Nylon 66, hybrid (20 per cent fiber by volume) with the fibers mixed together to form a random dispersion.
4. A 10 per cent short graphite/10 per cent polyaramid fiber reinforced Nylon 66, hybrid (20 per cent fiber by volume) laminated with alternate layers of the two fibers.

The nylon was a 60-80 mesh powder of DuPont's Zytel 101, supplied by Liquid Nitrogen Processing Corporation. The graphite fibers were Hercules, Inc., type AS, (see page 8). The polyaramid fibers were DuPont's Kevlar-49 type III, with 12.7 mm average length. The average diameter was 1.016×10^{-2} mm, the average ultimate tensile strength was 400,000 psi, the modulus of elasticity was 19×10^{6} psi and the density was 1.45 g/cc.

The composite samples contained 20% by volume of fiber in a random in-a-plane orientation and measured approximately 7.5 x 7.5 x 1/8 in. Polyaramid fibers were slurried in a tank of water using a hand mixer. The dilute mixture was stirred for three minutes and then allowed to rest for five minutes to permit settling of the fibers in the slurry. A rigid net at the bottom of the tank was then pulled upward catching the floating fibers and building up a mat of fibers with a random in-a-plane dispersion. A piece of filter paper was then placed over the fibers on the net and the mat was dried in place. The net was then separated from the filter paper, leaving a thin uniform random-in-a-plane veil of fibers. The essential feature of this operation is that the original polyaramid

fiber bundles of the chopped roving are broken up so that individual fibers are liberated and are free to act as individual elements of reinforcement. Without this process of liberation the composite properties are poor and the products are much less reproducible. One layer in the final composite material was made from 12 such veils cut to fill an area of 19 x 19 cm. One portion of nylon powder was then sprinkled evenly over the resulting layer. The procedure was repeated, placing one composite layer on top of the next until the proper thickness of composite sheet was attained. In order to make a hybrid laminated sandwich structure the layers of graphite fiber and PRD fiber were alternated. For the hybrid mixture, each layer consisted of a mixture of both graphite and polyaramid. The composite mats were then compression molded using the same technique reported previously (23).

The composites were annealed between heavy metal plates in a silicone oil bath at 185°C for 24 hours. In the process, internal stresses were relieved and the nylon developed a fixed percentage of crystallinity.

Cantilever beams for use in the crack propagation experiments were 3 inches by 1 inch by 1/8 inch. Precisely placed channels were cut in the center of each face parallel to the length of the specimen, forming a path for crack propagation with a width of 0.01 inches. A sharp crack 1.0 inch in length was cut into one side of the beam between the loading points.

The standard tensile bars for measurement of the breaking strength and the modulus of elasticity were used. They were 6.5 inches long by 1/2 inch wide. The ends of the dog-bone shape were 3/4 inch wide.

The test specimens were boiled for 24 hours in a 48% aqueous solution of potassium acetate. During this process the composite absorbed 2.8 per cent water which is equal to the equilibrium absorption in air at 55 per cent relative humidity. The equilibrium moisture content can be controlled at any other level by changing the salt concentration. The specimens were then stored at 55 per cent

relative humidity and room temperature in a glove box until they were tested. Test specimens conditioned at 100 per cent relative humidity were boiled in pure water for 30 hours and then stored under water.

2. Crack Propagation Rate Measurements

The compliance method was used to monitor crack length. The calibration was carried out by increasing the crack length in small steps of 0.02 to 0.035 of an inch with a jeweler's saw and recording the crack opening versus the applied load. The slope of each curve is the compliance for this specific crack length. The calculated compliance was plotted versus the crack length as in Figures B-1 to B-4 in Appendix B.

In order to record the crack opening at the points of load application during the cyclic fatigue crack propagation experiment, a sampling and hold circuit was installed into the peak monitoring section of the Instron 1230 Stress Function Generator. This sampling and hold device enabled continuous monitoring of the upper or lower peaks of the cyclic strain on a Houston strip chart recorder.

3. Data Analysis: Calculation of Stress Intensity Factor and Crack Propagation Rate

Continuous monitoring of the upper limit of stroke at the point of load application was obtained by feeding the stroke output signal into the sampling and hold device. The ratio of the upper limit of the stroke to the peak of the load amplitude could be calculated to produce the instantaneous compliance

$$C = \frac{U_{max}}{P_{max}} \qquad (18)$$

The change of the compliance with time for a specific cyclic loading condition was calculated by:

$$\frac{dC}{dt} = \frac{C_2 - C_1}{t_2 - t_1} \tag{19}$$

where t is the time.

The rate of crack propagation da/dt can be calculated from the compliance curve and the experimental data from the following equation

$$\frac{dC}{dt} = \frac{dC}{da} \times \frac{da}{dt}$$

or (20)

$$\frac{da}{dt} = \frac{dC}{dt} / \frac{dC}{da}$$

where dC/da was calculated from the derivative of the calibration curve. The derivative was obtained by fitting the data to a polynomial of the form:

$$C = A_o + A_1 \times a_i^{1/2} + A_2 \times a_i^{1.5} + \ldots + A_5 \times a_i^{4.5} \tag{21}$$

The constants were obtained using a Linear Regression Algorithm and then differentiating:

$$dC/da = 1/2 \times A_1 \times a_i^{-1/2} + 1.5 \times A_2 \times a_i^{1/2} + \ldots \ldots 4.5 \times A_5 \times a_i^{3.5} \tag{22}$$

The strain energy release rate G can be calculated from:

$$G = \frac{1}{2W} P^2 \frac{dC}{da} \tag{23}$$

where W is the width of the crack (which is narrower than the sample because of the machined grooves) and P is the applied load. Maximum and minimum values of G, ie., G_{max} and G_{min}, can be calculated by using the maximum and minimum values of the applied cyclic load, P_{max} and P_{min}.

The plane strain stress intensity factor K can then be computed:

$$K = [G E / (1 - \nu^2)]^{1/2} \tag{24}$$

4. Mechanical Testing Results

(a) Tensile Properties

Tensile properties are reported for four different composites, which will be given the following designations:

20GR55RH - Nylon 66 containing 20 per cent by volume graphite fibers annealed for 24 hours, conditioned at 55 per cent relative humidity

PR55RH - Nylon 66 containing 20 per cent by volume polyaramid fibers annealed for 24 hours, conditioned at 55 per cent relative humidity

HYL55RH - Nylon 66 containing 20 per cent by volume graphite and polyaramid fibers, (each fiber 10%), annealed for 24 hours, conditioned at 55 per cent relative humidity

HYL100RH - Same composition as HYL55RH, annealed for 24 hours and conditioned at 100 per cent relative humidity

The theoretical and experimental breaking strength and modulus of elasticity are compared in Table (9). The Tsai-Halpin equations (42) were used to calculate the theoretical modulus from constituent properties:

$$E_{com} = 3/8\ E_{11_{com}} + 5/8\ E_{22_{com}} \tag{25}$$

where

$$E_{11_{com}} = \frac{1 + 2\ (l/D)_f\ V_f\ \ E_f + 2(l/D)_f\ (1-V_f)\ E_m}{(E_f/E_m)(1-V_f) + 2(l/D)_f + V_f} \tag{26}$$

$$E_{22_{com}} = \frac{E_f(1 + 2V_f) + 2(1-V_f)\ E_m}{(E_f/E_m)(1-V_f) + 2 + V_f} \tag{27}$$

and

$(l/D)_f$ is the length to diameter ratio (i.e., the aspect ratio of the fibers.) E_m is the modulus of the matrix. E_f and V_f are the modulus and volume

TABLE 9

STRENGTHS AND MODULI OF THE COMPOSITES

	Strength psi		Moduli psi		Ultimate Elongation
	Theoretical	Experimental	Theoretical	Experimental	Experimental
GR55RH	30,213	18,371	2,343,209	1,237,028	0.02
PR55RH	28,880	18,346	1,620,679	1,232,554	0.022
HYL55RH	29,546	19,717	1,937,434	1,272,049	0.017
HYL100RH	29,013	15,2799	1,660,592	910,170	0.021

fraction of the fibers, respectively.

For the hybrid composites the theoretical modulus is assumed to be the volume fraction average of the two components. A schematic diagram of the hybrid composite is shown in Fig. 16. In each layer the fiber volume fraction is 0.2 while the overall volume fraction for each type of fiber is equal to 0.1.

E_{11} and E_{22} were calculated using the following equations:

$$1/E_{22_{com}} = \frac{0.5}{(E_{22})\,Gr} + \frac{0.5}{(E_{22})_{PRD}} \qquad (28)$$

$$(E_{11})_{com} = (E_{11})_{gr} \times 0.5 + (E_{11})_{prd} \times 0.5 \qquad (29)$$

The properties of the constituents are:

E_f (graphite) = 32 x 10^6psi

E_f (Kevlar) = 19 x 10^6 psi

E_m (Nylon) (55% RH) = 1.8 x 10^5 psi

E_m (Nylon) (100% RH) = 7.4 x 10^4 psi

$(1/D)_f$ (graphite) = 714

$(1/D)_f$ (Kevlar) = 1087

There are no reliable theories for predicting the theoretical strength of random-in-a-plane reinforced composites, but if we estimate that it should be roughly equal to one-third of the value predicted by the rule of mixture:

$$S = 1/3\,(S_f V_f + S_m\,(1-V_f)) \qquad (30)$$

We can get "theoretical" results for strength.

The properties of the constituents are:

S_m (55% RH) = 8.3 Kpsi

S_m (100% RH) = 6.3 Kpsi

S_f (graphite) = 420 Kpsi

S_f (PRD) = 400 Kpsi

The measured composite efficiency is defined as the ratio of the experimental to theoretical value of either the strength or modulus.

$$\zeta = \text{efficiency} = \frac{E_{exp}}{E_{theor}} \times 100$$

or, $$\zeta = \text{efficiency} = \frac{S_{exp}}{S_{theor}} \times 100 \qquad (31)$$

These values are tabulated in Table 10.

TABLE 10. THE STRENGTH AND MODULI EFFICIENCIES OF THE COMPOSITES

Material	Strength Efficiency	Modulus Efficiency
GR55RH	60.8%	50.8%
PR55RH	63%	76%
HYL55RH	66.7%	65.6%
HYL100RH	54.5%	54.8%

The composite efficiency is of the order of 50 to 70 per cent, which is typical for short fiber reinforced composite with fiber loadings of this order.

The composite's strength are ranked in the following order,

HYL55RH > GR55RH ≃ PR55RH > HYL100RH

The following order is valid for the modulus as well.

(b) Fatigue Crack Propagation

Cyclic fatigue tests were run on the same four materials mentioned before. All samples were run at 6 Hz. The damage propagation measurements were carried out under humidity conditions identical to those used for conditioning the samples, since it was observed that humidity changes greatly influenced the propagation rates. Samples conditioned at 100 per cent relative humidity were tested while over water, in a tank especially designed for this purpose.

Since the interaction of both the stress intensity range, ΔK, and the absolute value of the stress intensity factor as represented by K_{max} was sought, both values were changed during the course of the experiment.

An equation of the form suggested by Erdogen provided a suitable functional

formula for correlation of the data. This equation can be written as:

$$\dot{a} = A\, K_{max}^{m}\, \Delta K^{n} = A\, [K_{max}\, (1-R)^{n/n+m}]^{m+n} \qquad (32)$$

Taking the logarithms of both sides we obtained

$$\log \dot{a} = \log A + m \log K_{max} + n \log \Delta K \qquad (33)$$

A regression analysis was used to obtain the best values of m, n and A. Results for the four materials tested are given below:

GR55RH: $\dot{a}$ (cm/min) = $0.98 \times 10^{-51}\, [K_{max}\, (1-R)^{0.12}]^{17.87}$ (34)

with a correlation coefficient 0.924

PR55RH: $\dot{a}$ (cm/min) = $4.2 \times 10^{-9}\, [K_{max}\, (1-R)^{0.79}]^{2.44}$ (35)

with a correlation coefficient 0.915

HYL55RH: $\dot{a}$ (cm/min) = $1.31 \times 10^{-20}\, [K_{max}\, (1-R)^{0.25}]^{6.5}$ (36)

with a correlation coefficient 0.804

HYL100RH: $\dot{a}$ (cm/min) = $8.18 \times 10^{-13}\, [K_{max}\, (1-R)^{0.47}]^{2.85}$ (37)

with a correlation coefficient 0.908

K_{max} is in units of kg - $cm^{-3/2}$.

For a stress intensity factor value of 600 kg - $cm^{-3/2}$ and a value of R = 0.5, which is representative of the values used in the fatigue crack propagation experiments, the crack propagation rates are calculated:

GR55RH	9.8×10^{-3} (cm/min)
PR55RH	6.6×10^{-3} (cm/min)
HYL55RH	4.9×10^{-3} (cm/min)
HYL100RH	2.7×10^{-5} (cm/min)

which rank the resistance of the composites to crack propagation in the following order.

HYL100RH > HYL55RH ≃ PR55RH > GR55RH

The propagation rates are also plotted as a function of (1-R) at K_{max} = 645 kg - $cm^{-3/2}$ and as a function of K_{max} at R = 0.7 in Figures 17 and

18 respectively.

One may conclude the following:

1. The sensitivity of crack propagation rate to the amplitude of stress intensity (as represented by 1-R) increases as the material becomes more ductile.
2. The resistance of PRD fiber-reinforced nylon to crack propagation is translated to the hybrid composite. The material is stronger and tougher than the graphite reinforced composite with an equivalent amount of fiber and is about as stiff as the graphite reinforced material.
3. The sensitivity of crack propagation to K_{max} increases as the composite becomes more brittle.

3. Fractography Studies

The Cambridge Stereoscan Scanning Electron Microscope was used for fracture studies. The fracture surfaces produced in the two different experiments (i.e. tensile tests and fatigue crack propagation tests) were examined. Samples were first vacuum coated with a thin layer of carbon followed by a thin layer of gold, in order to prevent static charge build-up.

Specimens fractured in constant strain-rate tension exhibited a relatively brittle fracture as shown in Figures 19 to 21. Fibers extending out of the fracture surface are relatively short for graphite but relatively long for PRD. The pulled out fibers are mainly those which are not oriented parallel to the load direction. The pullout length to diameter ratios (calculated from pulled fibers that are oriented parallel to the load direction) are 6 and 15 for graphite and PRD respectively.

If one assumes that the critical aspect ratio is of the order of twice this value, one can estimate the shear strength at the interface using the shear lag analysis.

$$\tau = \frac{S_f}{2(1/D)_{fc}} \tag{38}$$

For graphite fiber

$$\tau = \frac{420,000}{2(12)} = 17.5 \text{ Kpsi} \tag{39}$$

For PRD fiber

$$\tau = \frac{400,000}{2(30)} = 6.67 \text{ Kpsi} \tag{40}$$

The shear strength between graphite and nylon is of the order of the shear strength of the nylon matrix. This indicates that the adhesion of the nylon to the graphite fibers is good. On the other hand, the adhesion of the nylon to the PRD fibers is poor. Eagles (45) found that the interfacial bond strengths and frictional shear strength of unfinished PRD with nylon 12 was 6640 psi and 292 psi, respectively.

In samples fractured by cyclic fatigue (Figures 22 and 23), the aspect ratio is lower than in the tensile test specimens. Moreover, one can see in Figure 23 that the nylon matrix exhibited a high degree of yielding and a high degree of adhesion to the fibers.

In the PRD reinforced nylon composite, the early damage occurs near fibers lying perpendicular to the stress direction. The damage took place in the form of debonding (i.e. separation between the fiber and the matrix) that intensified progressively, affecting fibers at smaller angles to the applied load until at some higher load (less than the ultimate load) resin cracks occurred in the resin rich zone of the material.

For graphite reinforced nylon composites a similar mechanism is suggested. The only difference is that because of the good adhesion between the matrix and the fibers, the resin tends to draw in the direction of the stress.

VII. CONCLUSIONS

1. Both the fatigue lives and tensile strengths of short graphite fiber reinforced nylon 66 can be characterized by extreme value statistics. Modified Weibull functions may be used to describe the cumulative distributions for these two properties. The quality of a particular fabrication process can be evaluated by measuring the various moments of these distributions.

2. The mechanism of fatigue failure in graphite fiber reinforced nylon is shown to be influenced by the technique of fabrication of the composite. The compression molded materials were linearly elastic and exhibited an isothermal, brittle fatigue failure through initiation and propagation of cracks. The injection molded materials were non-linear and exhibited considerable ductile flow prior to ultimate failure. Continuous heating of the material resulted in premature failure, suggesting a thermal mode of failure.

3. For a specific population produced by one fabrication process using the same raw materials for each member of the population, there exists a unique relation between the cumulative distribution of tensile strengths and the cumulative distribution of fatigue lifetimes. Thus if the effect of an environmental variable on the distribution of strength is measured, the effect on the fatigue lifetime can be estimated.

4. Since the rate of crack propagation in graphite reinforced nylon is highly sensitive to stress (proportional to the 15th - 20th power of stress), the prediction of fatigue lifetime directly from crack propagation data is highly unreliable.

5. The mechanism of crack propagation in short graphite fiber reinforced nylon is phenomenologically similar to the growth and fracture of crazes in thermoplastics. The propagation of damage at a crack tip is controlled by matrix deformation, cavitation, fiber breakage and fiber pullout. Damage can propagate in the absence of crack growth until a critical point is reached at which time the material fractures catastrophically.

6. Hybrid composites of polyaramid fibers and graphite fibers are more resistant to crack propagation than graphite composites with an equivalent fiber content. The toughness attributed to the polyaramid fibers is translated directly into the composite. Increased ductility increases the sensitivity of the fatigue crack propagation rate to the amplitude of the stress intensity factor while decreasing its sensitivity to the maximum stress intensity factor.

ACKNOWLEDGEMENT

This research is being sponsored by The Army Materials and Mechanics Research Center, Watertown, Massachusetts, with Dr. R. W. Lewis and Dr. M. Roylance as Technical Supervisors.

VIII. References

1. Broutman, L. J., S. Sahu, "Progressive Damage of a Glass Reinforced Plastic During Fatigue" 24th ANTEC Reinforced Plastics/Composites Division SPI, Section 11-D.
2. McGarry, F. J., M. B. Desai, "Failure Mechanisms in Glass Reinforced Plastics" ASTM Bulletin 239, 76, (1959).
3. Dally, J. W., D. H. Carrillo, Poly. Eng. Sci. 9, 434 (1969).
4. Manson, J. A., R. W. Hertzberg, "Fatigue Failure in Polymers", Crit. Rev. Macromole. Sci. 1, 433 (1973).
5. Di Benedetto, A. T., J. V. Gauchel, R. L. Thomas, J. W. Barlow, J. Materials, 7 (2), 211, (1972).
6. Owen, M. J., R. J. Howe, J. Phys. (D) 5, 1637 (1972).
7. Irwin, G. R., Fracture Toughness Testing of High Strength Sheet Materials Under Conditions Appropriate for Stress Analysis, Naval Research Laboratory Report 5486 (1960).
8. Paris, P. C., G. C. M. Sih, "Stress Analysis of Cracks" Spec. Tech. Publ. 381, ASTM 30 (1965).
9. Dugdale, J., Mech. Phys. Solids 8, 100 (1960).
10. Cessna, L. C., S. S. Sternstein, in Fundamental Phenomena in Materials Science 4, 45 (1966) Plenum Press, N.Y.
11. Knauss, W. G., Inter. J. Fracture Mech. 6 (1), 7 (1960).
12. Wnuk, M. P., Inter. J. Fract. 10 (2), 223 (1974).
13. Schapery, R. A., Inter. J. Fract. 11 (1) 141, (3) 369, (4) 549, 1975.
14. Kitigawa, M., K. Motomura, J. Poly. Sci., 12 (1974).
15. Thornton, P. A., J. Comp. Mat. 6, 147 (1972).
16. Di Benedetto, A. T., K. C. Trachte, Int. J. Poly. Mat. 1, 75 (1971).
17. Owens, M. J., P. T. Bishop, J. Physics, D 7, 1214 (1974).
18. Epstein, B., J. Appl. Phys. 19, 140 (1948).

19. Bury, K. V., Statistical Models in Applied Science, J. Wiley & Sons, N.Y. (1975).

20. Rosen, B. W., C. H. Zweben, NASA Contractor Report NASA-CR-2057, August (1972).

21. Halpin, J. C., J. R. Hopf, W. Goldberg, J. Comp. Mat. 4, 462 (1970).

22. Halpin, J. C., J. Comp. Mat. 6, 208 (1972).

23. Di Benedetto, A. T., G. Salee, R. Hlavacek, Poly. Eng. Sci., 15 (4), 242 (1975).

24. Hahn, H. T., R. Y. Kim. J. Comp. Mat. 9, 297 (1975).

25. Knight, M., H. T. Hahn, J. Comp. Mat. 9, 77 (1975).

26. Freudenthal, A. M., E. J. Gumbel, Trans. Roy. Soc. Lond. Ser. A216, 309 (1953).

27. Pelloux, R. M. N., Review of Theories and Laws of Fatigue Crack Propagation, AFFDL-TR-70-144, Proceedings of the Air Force Conf. on Fatigue of Aircraft Structures and Materials pp. 404-16 (1970).

28. Hoeppner, D. W., W. E. Krupp, Eng. Fract. Mech. 6, 47 (1974).

29. Salee, G., "Fatigue Behavior of Graphite Fiber Reinforced Nylon 66 Composites", Ph.D Dissertation, University of Connecticut (1976).

30. Erdogen, F., "Crack Propagation Theories, An Advanced Treatise" Academic Press, N.Y. (1968).

31. Owens, M. J., P. T. Bishop, J. Physics, D, 7 1214 (1974).

32. Mandell, J. F., F. J. McGarry, S. S. Wang, T. Im, J. Comp. Mat. 8, 106 (1974).

33. Gaggar, S., L. J. Broutman, J. Comp. Mat. 9, 216 (1975).

34. Di Benedetto, A. T., A. D. Wambach, Int. J. Poly. Mat. 1, 159 (1972).

35. Holdsworth, A. W., S. Morris, M. J. Owen, J. Phys. D, 7, 2036 (1974).

36. McGarry, F. J., J. F. Mandell, Proc. 27th Reinforced Plastics Composites Div. SPI (1972) Section 9-A.

37. Harris, B., J. Morley, D. C. Phillips, J. Mat. Sci. 10, 2050 (1975).

38. Gaggar, A., L. J. Broutman, Int. J. Fract. 10, 606 (1974).

39. Broutman L. J., S. Sahu, S.T.P. 497, ASTM (1972).

40. Agarwal, B. D., J. W. Dally, J. Mat. Sci., 10, 193 (1975).

41. Halpin, J. C., K. L. Jerina, T. A. Johnson, Characterization of Composites for the Purpose of Reliability Evaluation, Tech. Report AFL TR-73-289, Dec. (1972).

42. Ashton, J. E., J. C. Halpin, P. H. Petit, "Primer on Composite Materials: Analysis" p 77-87, Technomic Pub., Stamford, Ct. (1969).

43. Marshall, G. P., L. E. Culver, J. G. Williams, Plastics and Polymers, 95-101 April (1970).

44. Owens, M. J., R. Dukes, J. Strain Anal. 2, 272 (1967).

45. Eagles, D.B., B.F. Blumentritt, S. L. Cooper, J. App. Poly. Sci., 20 435 (1976).

TECHNICAL REPORT DISTRIBUTION

No. of Copies	To
1	Office of the Director, Defense Research and Engineering, The Pentagon, Washington, D. C. 20301
12	Commander, Defense Documentation Center, Cameron Station, Building 5, 5010 Duke Street, Alexandria, Virginia 22314
1	Metals and Ceramics Information Center, Battelle Memorial Institute, 505 King Avenue, Columbus, Ohio 43201
	Chief of Research and Development, Department of the Army, Washington, D. C. 20310
2	ATTN: Physical and Engineering Sciences Division
	Commander, Army Research Office (Durham), Box CM, Duke Station, Durham, North Carolina 27706
1	ATTN: Information Processing Office
	Commander, U. S. Army Materiel Command, 5001 Eisenhower Avenue, Alexandria, Virginia 22333
1	ATTN: AMCRD-TC
	Commander, Deseret Test Center, Fort Douglas, Utah 84113
1	ATTN: Technical Information Office
	Commander, U. S. Army Electronics Command, Fort Monmouth, New Jersey 07703
1	ATTN: AMSEL-GG-DD
1	AMSEL-GG-DM
	Commander, U. S. Army Missile Command, Redstone Arsenal, Alabama 35809
1	ATTN: Technical Library
1	AMSMI-RSM, Mr. E. J. Wheelahan
	Commander, U. S. Army Armament Command, Rock Island, Illinois 61201
2	ATTN: Technical Library
1	AMSAR-SC, Dr. C. M. Hudson
1	AMSAR-PPW-PB, Mr. Francis X. Walter
	Commander, U. S. Army Natick Laboratories, Natick, Massachusetts 01760
1	ATTN: Technical Library
	Commander, U. S. Army Satellite Communications Agency, Fort Monmouth, New Jersey 07703
1	ATTN: Technical Document Center
	Commander, U. S. Army Tank-Automotive Command, Warren, Michigan 48090
2	ATTN: AMSTA-BSL, Research Library Branch

No. of Copies	To
	Commander, Aberdeen Proving Ground, Maryland 21005
1	ATTN: STEAP-TL, Bldg. 305
	Commander, Frankford Arsenal, Philadelphia, Pennsylvania 19137
1	ATTN: Library, H1300, Bl. 51-2
1	SMUFA-L300, Mr. Harold Markus
	Commander, Harry Diamond Laboratories, Connecticut Avenue and Van Ness Street, N. W., Washington, D. C. 20438
1	ATTN: Technical Information Office
	Commander, Picatinny Arsenal, Dover, New Jersey 07801
1	ATTN: SMUPA-RT-S
1	SARPA-FR-M-D, PLASTEC, A. M. Anzalone
	Commander, Redstone Scientific Information Center, U. S. Army Missile Command, Redstone Arsenal, Alabama 35809
4	ATTN: AMSMI-RBLD, Document Section
	Commander, Watervliet Arsenal, Watervliet, New York 12189
1	ATTN: SWEWV-RDT, Technical Information Services Office
	Commander, U. S. Army Foreign Science and Technology Center, 220 7th Street, N. E., Charlottesville, Virginia 22901
1	ATTN: AMXST-SD3
	Director, Eustis Directorate, U. S. Army Air Mobility Research and Development Laboratory, Fort Eustis, Virginia 23604
1	ATTN: Mr. J. Robinson, SAVDL-EU-SS
	Librarian, U. S. Army Aviation School Library, Fort Rucker, Alabama 36360
1	ATTN: Building 5907
	Commander, U. S. Army Engineer Waterways Experiment Station, Vicksburg, Mississippi 39180
1	ATTN: Research Center Library
	Commander, U. S. Army Environmental Hygiene Agency, Edgewood Arsenal, Maryland 21010
1	ATTN: Chief, Library Branch
	Naval Research Laboratory, Washington, D. C. 20375
1	ATTN: Dr. J. M. Krafft - Code 8430
	Chief of Naval Research, Arlington, Virginia 22217
1	ATTN: Code 471

No. of Copies	To
	Air Force Materials Laboratory, Wright-Patterson Air Force Base, Ohio 45433
2	ATTN: AFML (LAE), E. Morrissey
1	AFML (LC)
1	AFML (LMD), D. M. Forney
	National Aeronautics and Space Administration, Washington, D. C. 20546
1	ATTN: Mr. B. G. Achhammer
1	Mr. G. C. Deutsch - Code RR-1
	National Aeronautics and Space Administration, Marshall Space Flight Center, Huntsville, Alabama 35812
1	ATTN: R-P&VE-M, R. J. Schwinghamer
1	S&E-ME-MM, Mr. W. A. Wilson, Building 4720
1	Materials Sciences Corporation, Blue Bell Campus, Merion Towle Building, Blue Bell, Pennsylvania 19422
	Lockheed-Georgia Company, Marietta, Georgia 30060
1	ATTN: Advanced Composites Information Center, Dept. 72-14 - Zone 402
1	Dr. John Mandell, Massachusetts Institute of Technology, Cambridge, Massachusetts 02139
1	Dr. Richard Hertzberg, Lehigh University, Bethlehem, Pennsylvania 18015
1	Dr. Lawrence Broutman, Illinois Institute of Technology, 3300 S. Federal St., Chicago, Illinois 60616
1	Dr. Ken Hofer, Illinois Institute of Technology Research Institute, 10 West 35th St., Chicago, Illinois 60616
1	Dr. Michael Salkind, United Aircraft Corp., Sikorsky Division, Stratford, Connecticut 06602
	Director, Army Materials and Mechanics Research Center, Watertown, Massachusetts 02172
2	ATTN: DMXMR-PL
1	DMXMR-PR
1	DMXMR-CT
1	DMXMR-AP
1	DMXMR-R, Dr. Thomas
1	DMXMR-RD, Dr. Lewis
4	DMXMR-RD, Mrs. Roylance

FIG. 1 CUM. DIST. OF STRENGTH

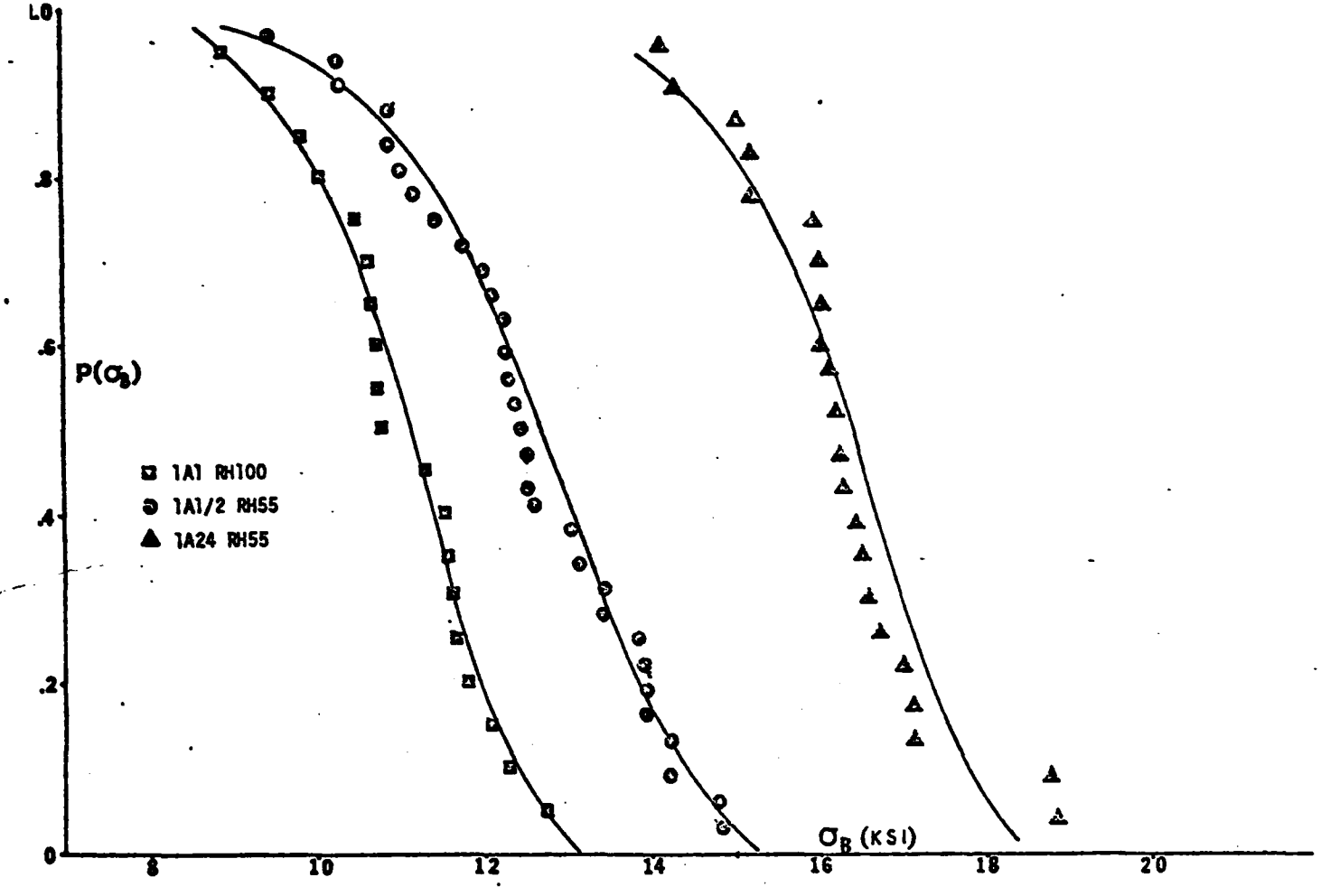

Figure 2. Cumulative Distributions of Breaking Stress

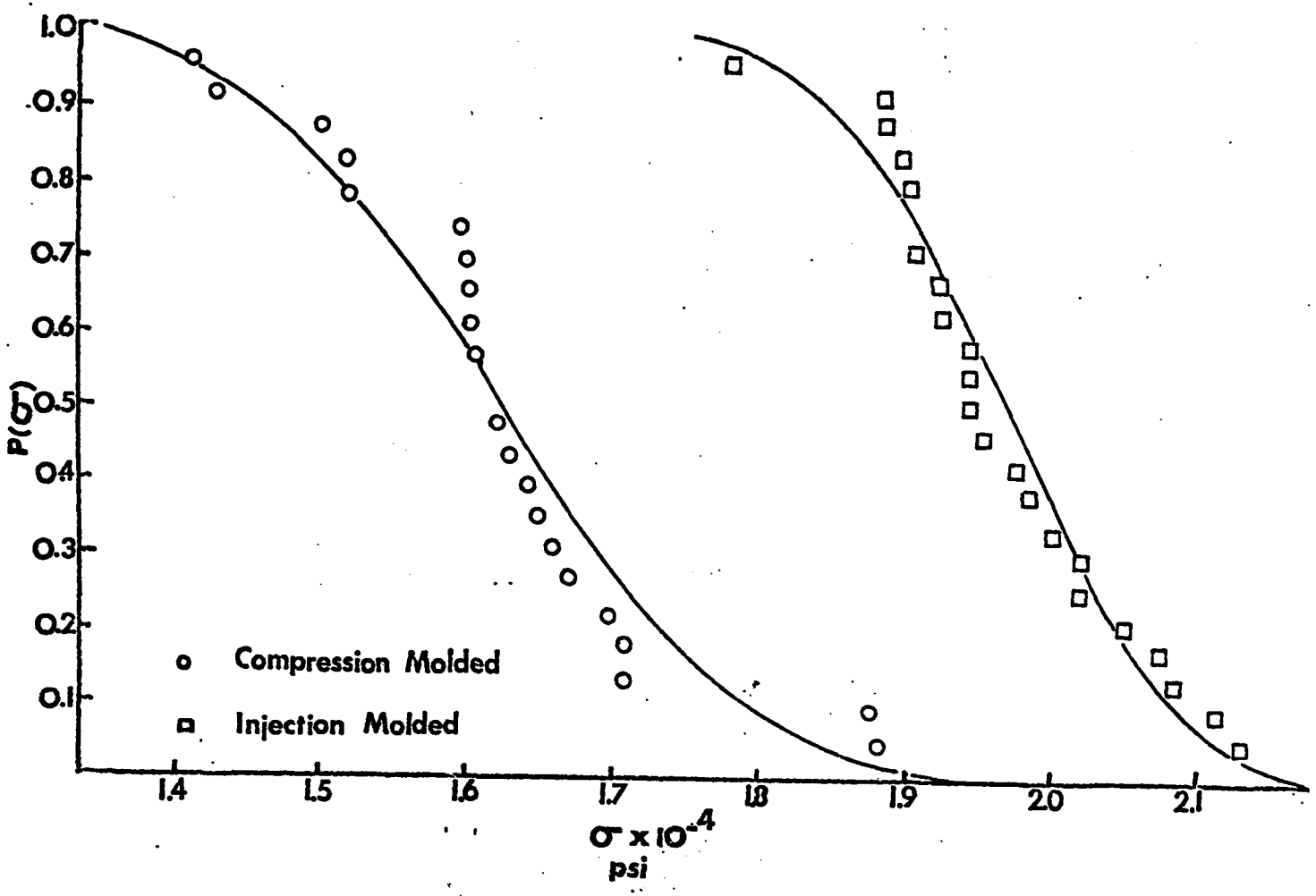

Figure 3. Cumulative Distribution of Fatigue Lines

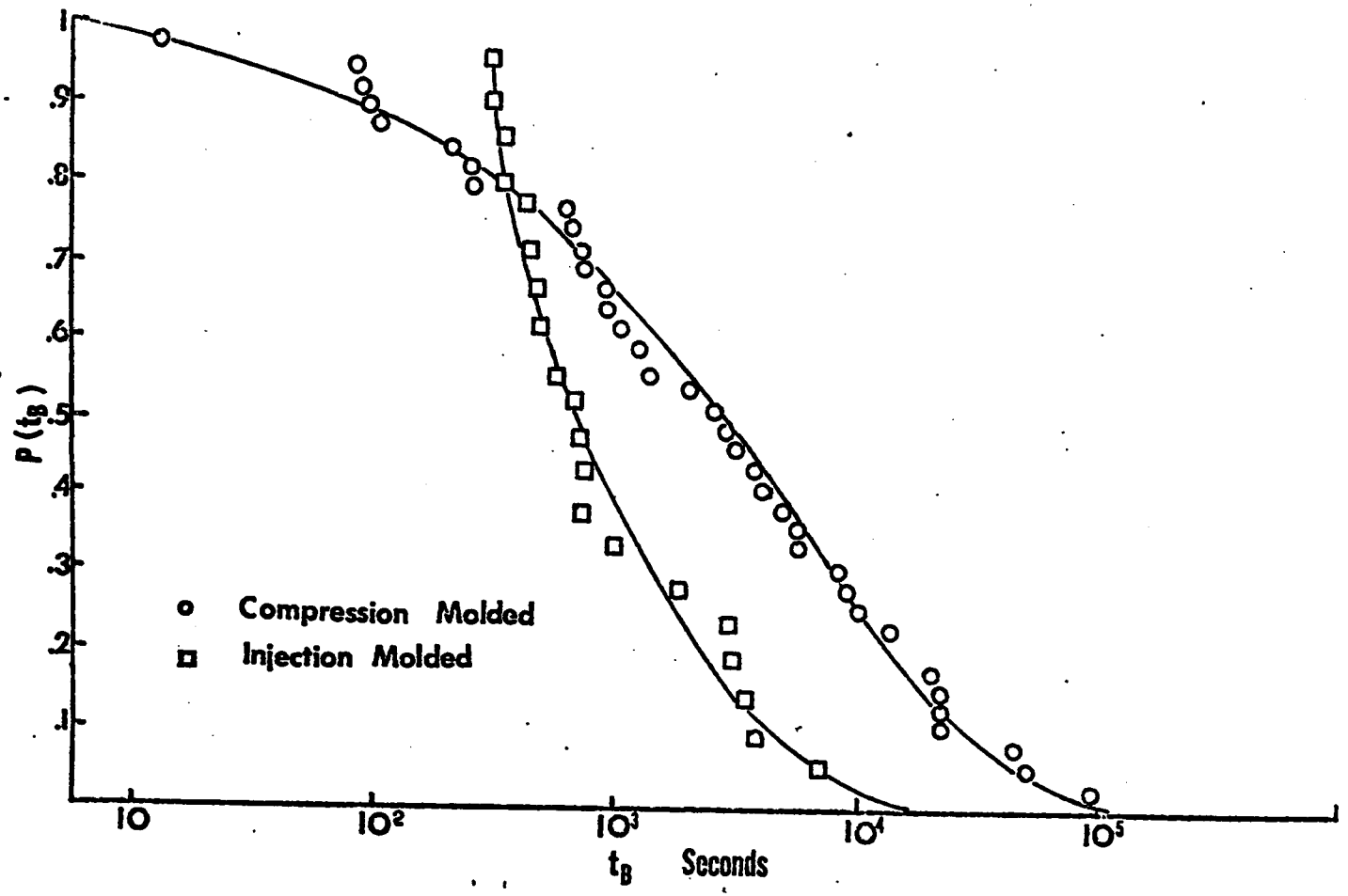

FIG. 4. CUM. DIST. OF FATIGUE LIFE

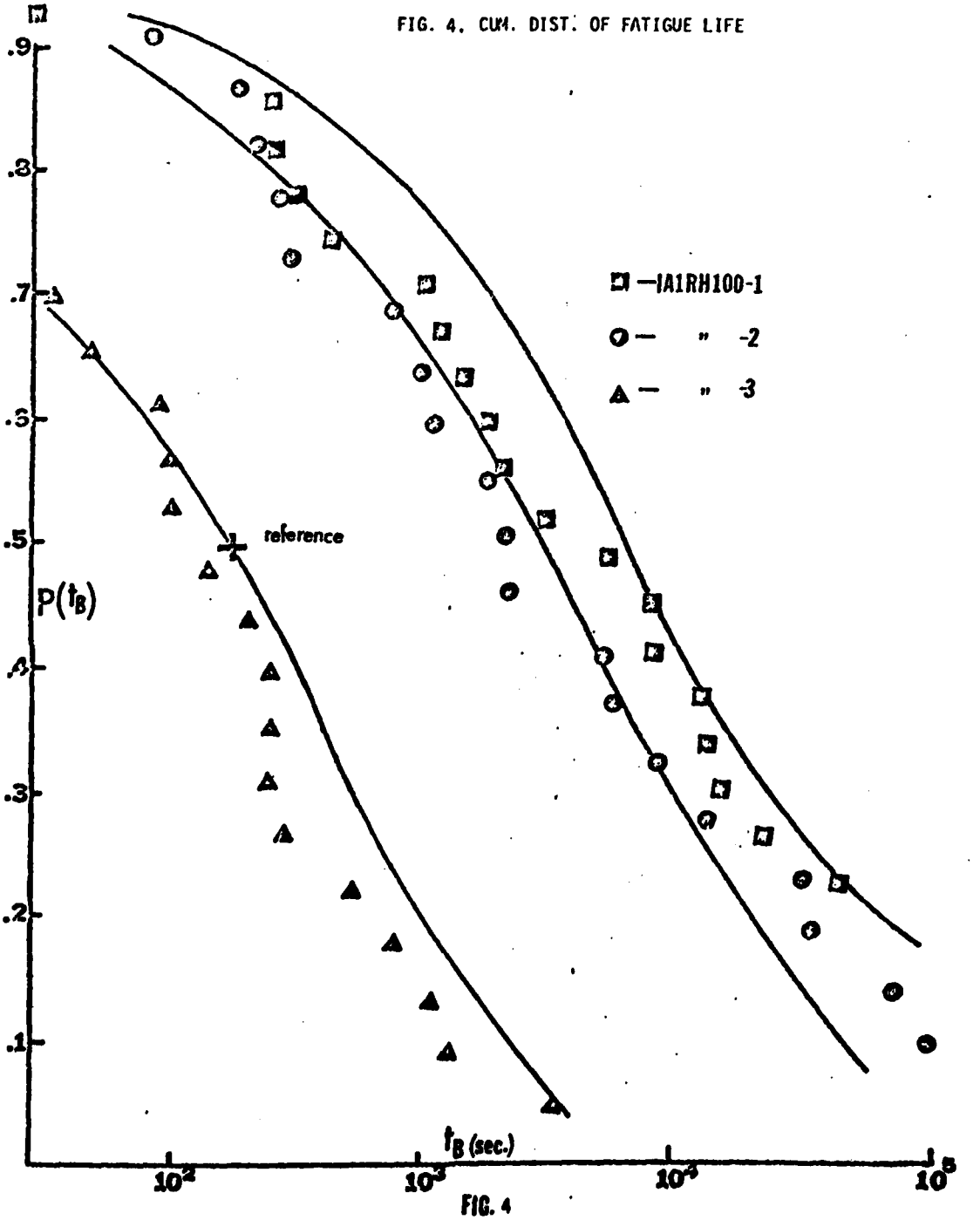

FIG. 4

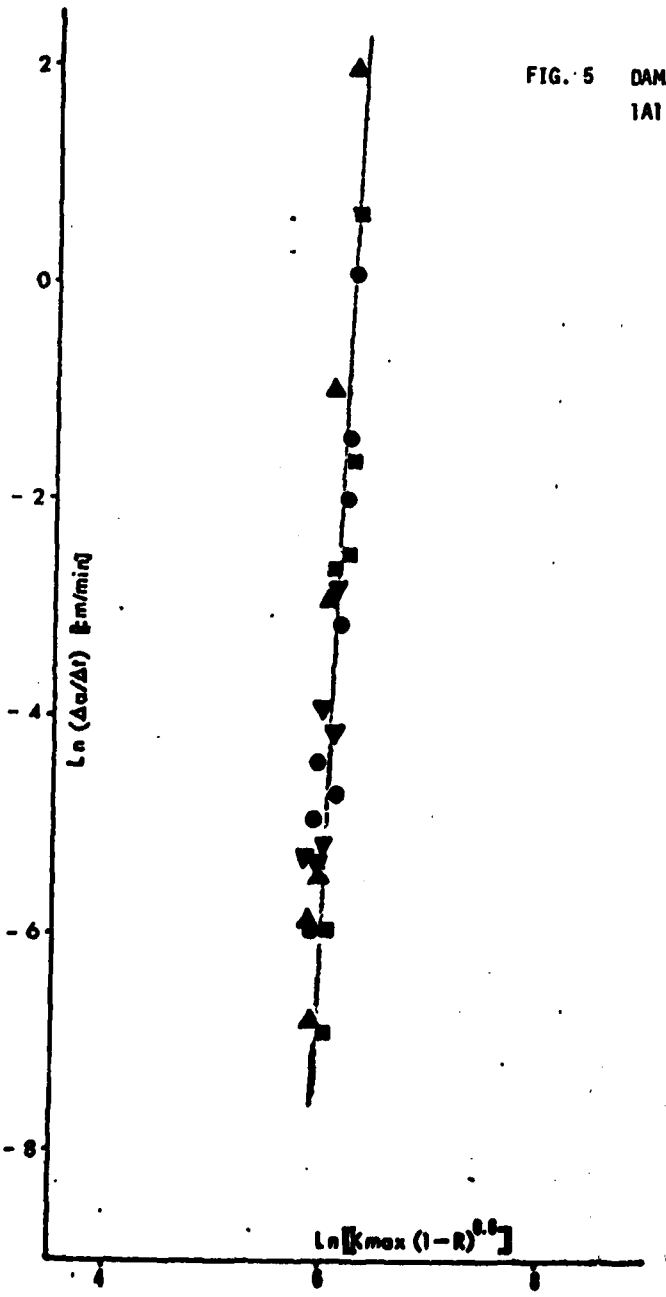

FIG. 5 DAMAGE PROPAGATION RATE FOR 1AI RH100

FIG. 6 DAMAGE PROPAGATION RATE FOR 1A1 RH100 (EXPANDED SCALE)

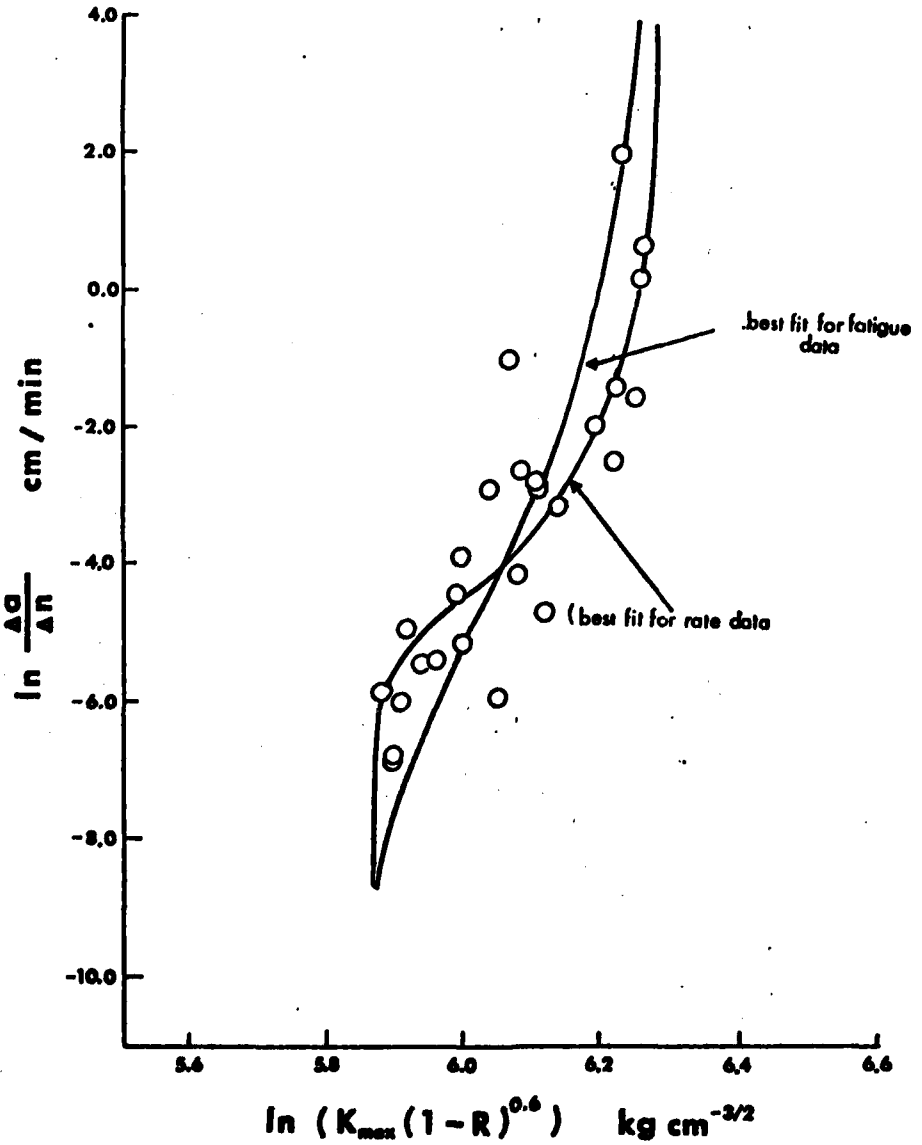

FIG. 7 MASTER CURVE - STRENGTH VS FATIGUE LIFE

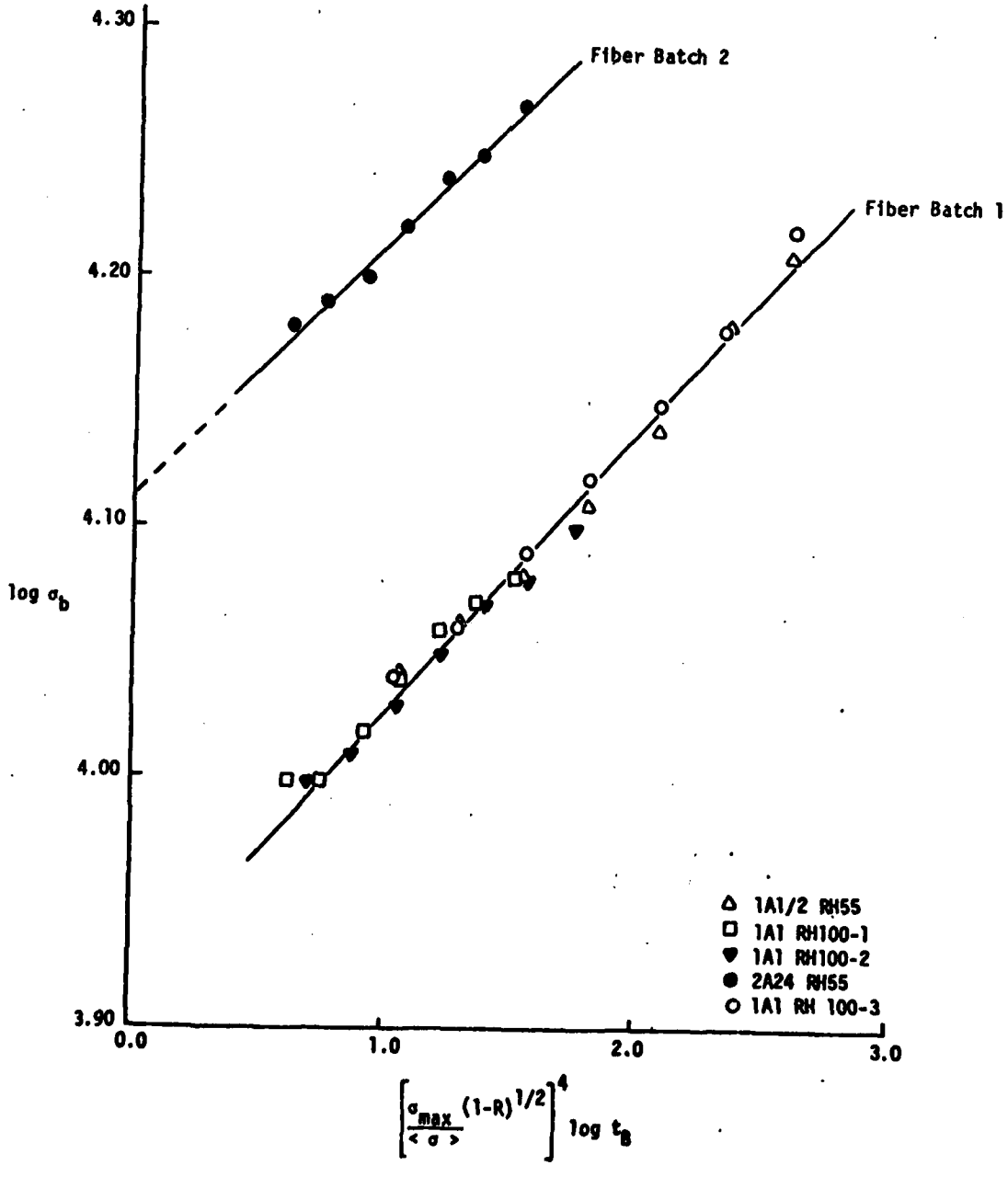

FIG. 8 CUM. DIST. OF FATIGUE LIFE

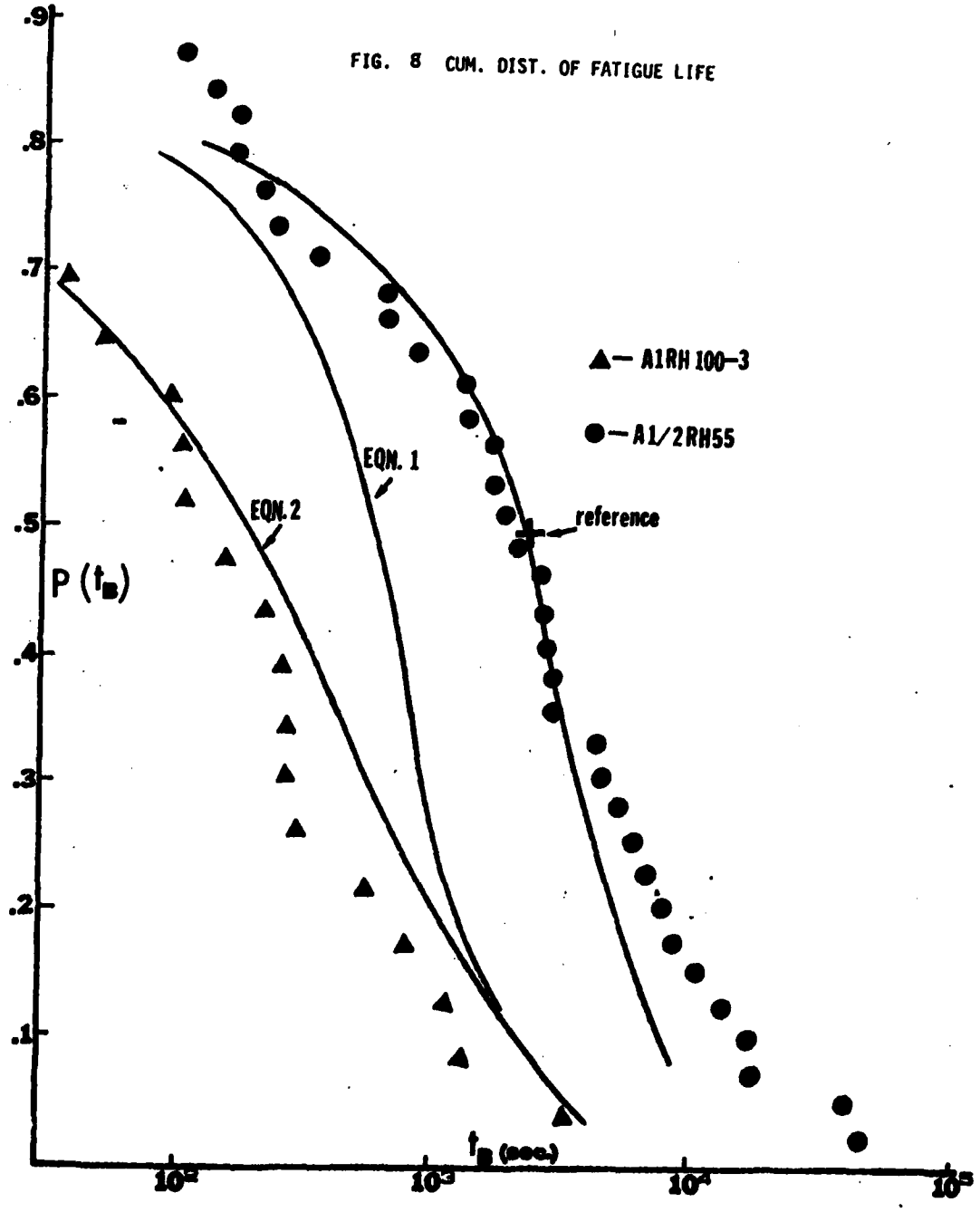

FIG. 9 FATIGUE FAILURE SURFACE -
RESIN DRAWN NORMAL TO FIBER

FIG. 10 FATIGUE FAILURE SURFACE - CAVITATION AND STRIATIONS AROUND FIBER END

Figure 11 Tracing of Strip Chart Recording of Temperature Change During Fatigue

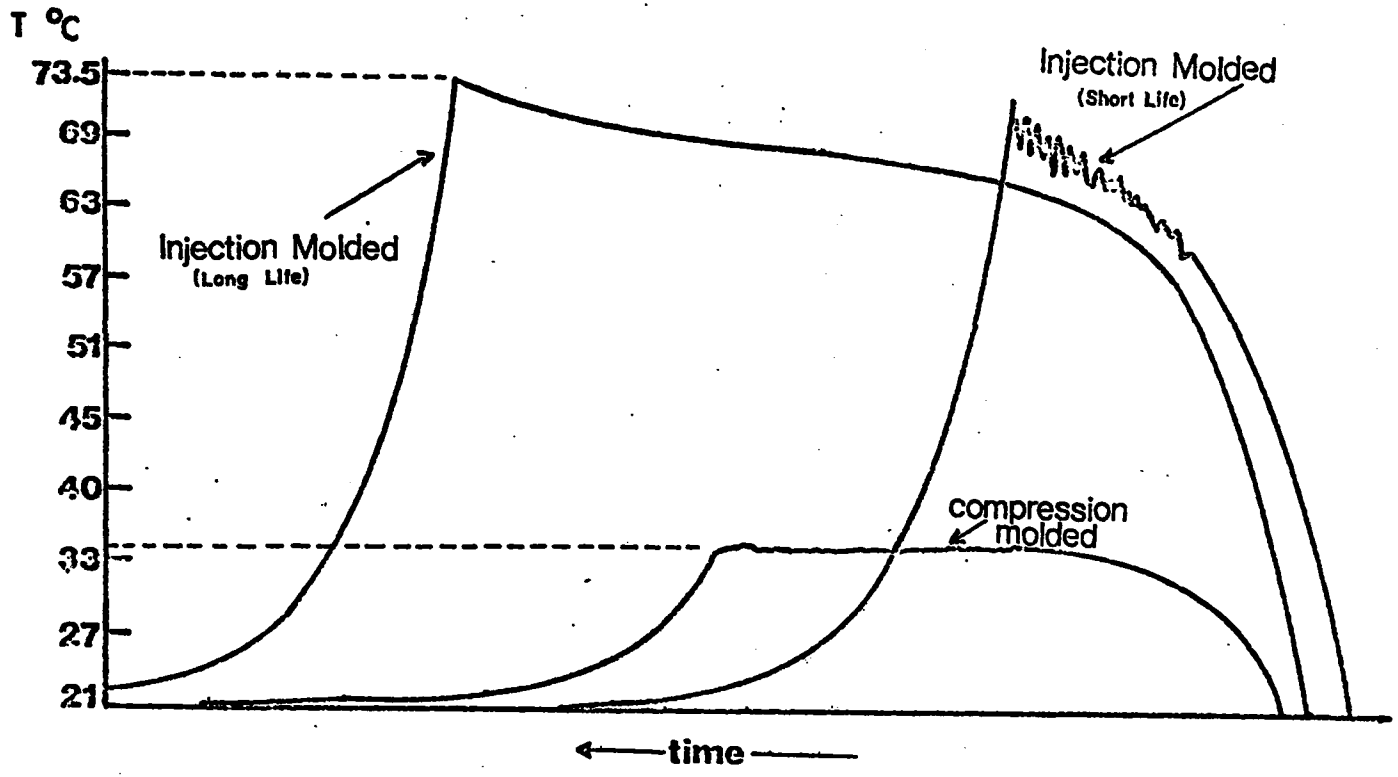

FIGURE 12 SEM Photograph of the Fracture Surface of a Compression Molded Specimen

FIGURE 13 SEM Photograph of the Fracture Surface of an Injection Molded Specimen

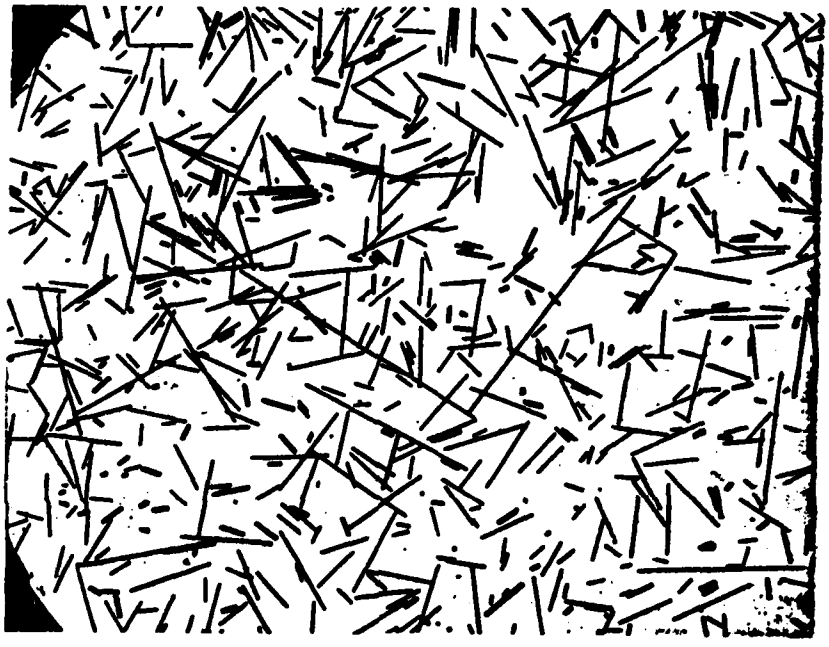

Figure 14. Fiber length distribution for injection molded specimens.

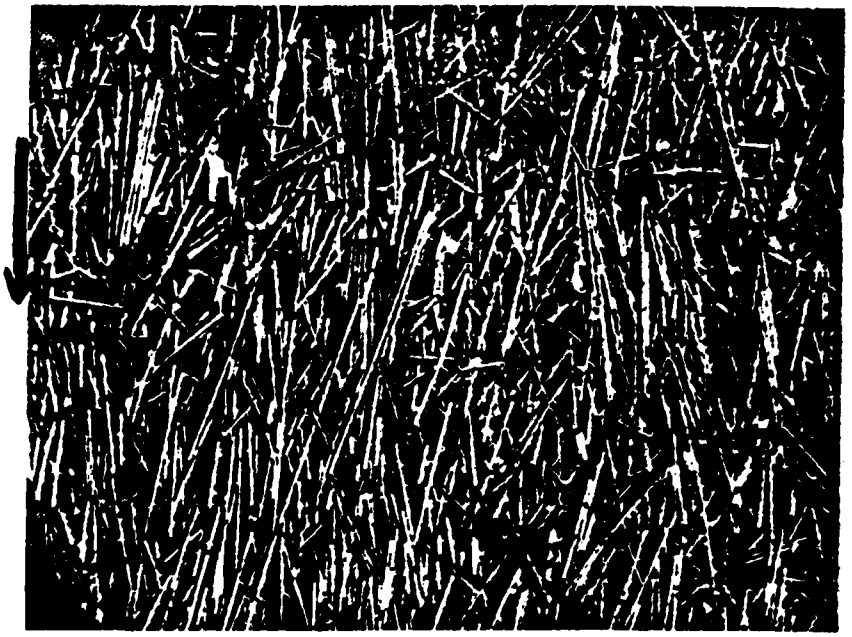

FIGURE 15. DARK FIELD PHOTOGRAPH OF ORIENTED FIBERS IN INJECTION MOLDED SPECIMENS

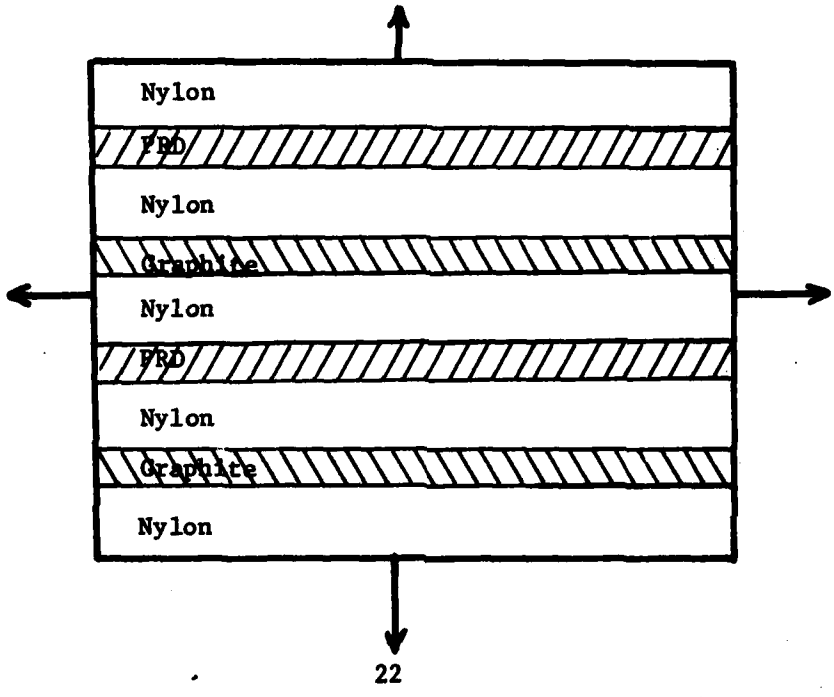

Fig. 16. Schematic Structure of Hybrid lamina composite

Fig. 17. Crack Propagation Velocity vs 1-R

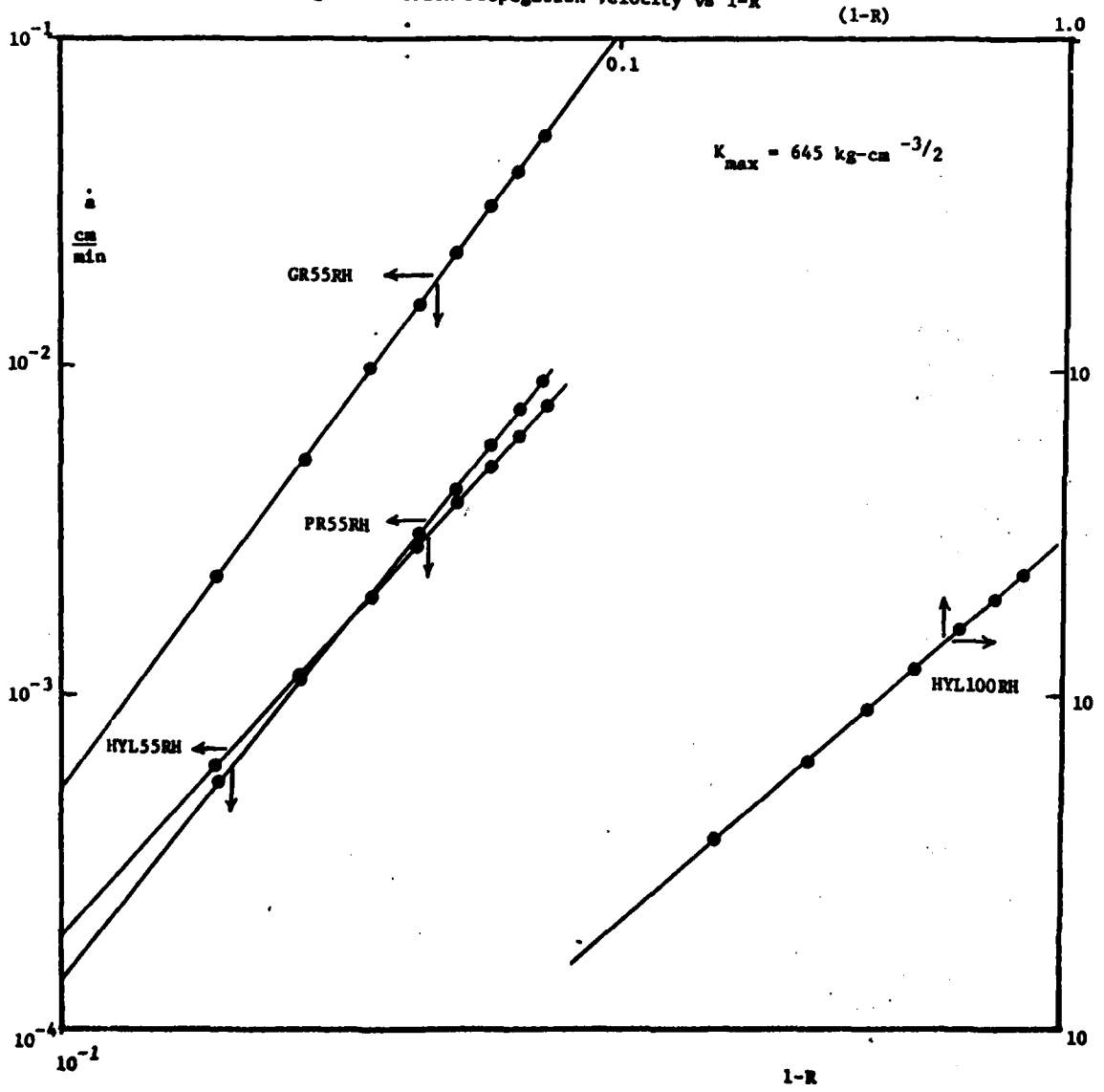

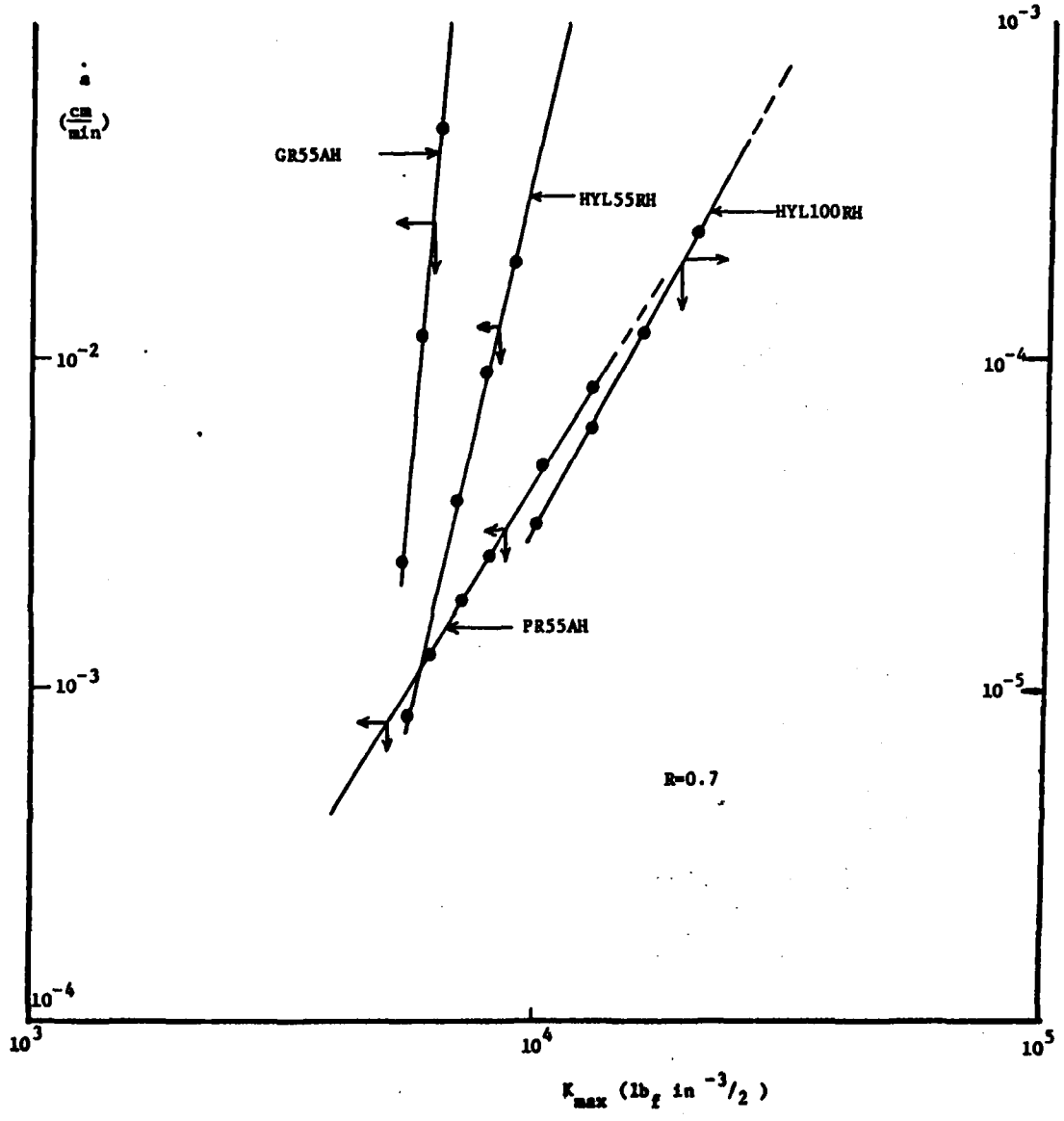

Fig. 18. Crack Propagation Velocity vs Maximum Stress Intensity Factor

Fig.19 . Fracture Surface of PR55RH Tested in Tension (x1000)

Fig. 20. Fracture Surface of GR55RH Tested in Tension (x500)

Fig. 21. Fracture Surface of HY100kll Tested in Tension (x100)

Fig. 22. Fracture Surface of PR55RH Tested in Fatigue (x180)

Fig. 23 Fracture Surface of GR55RH Tested in Fatigue (x700)

APPENDIX

TABLE A-1

Breaking Strength Distribution
Population Annealed for 1/2 Hr
Conditioned at 55% RH

Fraction Surviving	Breaking Stress (psi)
0.97	9,450
0.94	10,242
0.91	10,247
0.88	10,868
0.84	10,868
0.81	11,000
0.78	11,173
0.75	11,401
0.72	11,750
0.69	12,000
0.66	12,100
0.63	12,215
0.59	12,215
0.56	12,260
0.53	12,333
0.50	12,414
0.47	12,500
0.44	12,500
0.41	12,571
0.38	13,012
0.34	13,100
0.31	13,406
0.28	13,406
0.25	13,810
0.22	13,899
0.19	13,900
0.16	13,900
0.13	14,201
0.09	14,206
0.06	14,770
0.03	14,821

Table A-2

Breaking Strength Distribution. Population Annealed for 1 Hour Conditioned at 55% RH

Fraction Surviving	Breaking Stress (p. s. i.)
0. 94	9465
0. 89	10052
0. 83	10572
0. 78	10671
0. 72	10704
0. 67	11084
0. 61	11350
0. 56	11669
0. 50	12176
0. 44	12413
0. 39	12566
0. 33	12588
0. 28	12727
0. 22	12725
0. 17	12801
0. 11	13220
0. 06	14053

Table A-3

Breaking Strength Distribution. Population Annealed for 1 Hour Conditioned at 100% RH

Fraction Surviving	Breaking Stress (p. s. i.)
0. 95	3897
0. 90	9445
0. 85	9830
0. 80	10027
0. 75	10476
0. 70	10607
0. 65	10645
0. 60	10642
0. 55	10701
0. 50	10755
0. 45	11240
0. 40	11519
0. 35	11550
0. 30	11607
0. 25	11628
0. 20	11769
0. 15	12055
0. 10	12278
0. 05	12723

Table A-4

Breaking Strength Distribution Population Annealed for 24 Hours Conditioned at 55% RH

Fraction Surviving	Breaking Stress (p. s. i.)
0. 96	14103
0. 91	14230
0. 87	15016
0. 83	15177
0. 78	15177
0. 74	15933
0. 70	15985
0. 65	16000
0. 60	16000
0. 57	16080
0. 52	16160
0. 47	16200
0. 43	16295
0. 39	16410
0. 35	16480
0. 30	16570
0. 26	16700
0. 22	16989
0. 17	17081
0. 13	17090
0. 09	18760
0. 04	18845

Table A-5

Breaking Strength Distribution Injection Molded Population Annealed for 24 Hours Conditioned at 55% RH

Fraction Surviving	Breaking Stress (p. s. i.)
0. 95	17941
0. 91	18831
0. 86	18855
0. 82	18952
0. 77	19025
0. 73	19073
0. 68	19073
0. 63	19218
0. 59	19235
0. 55	19436
0. 50	19436
0. 45	19767
0. 41	19324
0. 36	20039
0. 32	20195
0. 27	20211
0. 23	20573
0. 18	20735
0. 14	20840
0. 09	21155
0. 05	21324

TABLE A-6

Breaking Time Distribution - A 1/2 RH55
Specimens Annealed for Half an Hour
Conditioned at 55% R.H.

max = 11250 psi
Zero time breaks = 4

P(t)	t (Seconds)
0.872	100
0.846	130
0.821	160
0.795	160
0.769	200
0.744	230
0.718	340
0.692	620
0.667	630
0.641	830
0.615	1280
0.590	1290
0.564	1650
0.538	1680
0.513	1830
0.487	2070
0.462	2590
0.436	2610
0.410	2690
0.385	2980
0.359	3010
0.333	4400
0.308	4580
0.282	5340
0.256	6020
0.231	6410
0.205	7850
0.179	8540
0.154	10430
0.128	13400
0.103	17130
0.077	17440
0.051	39560
0.026	4482

TABLE A-7

Breaking Time Distribution - AlRH100-1
Specimens Annealed for One Hour
Conditioned at 100% R.H.

σ_{max} = 9061 psi
Zero Time Breaks = 1
Infinite Time Breaks = 4

$P(t_B)$	t_B (Seconds)
0.926	29
0.889	81
0.852	261
0.815	274
0.778	323
0.741	454
0.704	1009
0.667	1231
0.630	1580
0.593	1944
0.556	2250
0.519	3339
0.481	5998
0.444	8583
0.407	8614
0.337	13474
0.333	14550
0.296	15987
0.259	23386
0.222	46355
0.185	65421

TABLE A-8

Breaking Time Distribution-AlRH100-2
Specimens Annealed for One Hour
Conditioned at 100% R.H.

∇_{max} = 9279 psi
Zero time breaks = 1
Infinite time breaks = 1

$P(t_B)$	t_B (Seconds)
0.909	84
0.864	192
0.818	229
0.773	282
0.727	312
0.682	792
0.636	1033
0.591	1176
0.545	1974
0.500	2283
0.455	2350
0.409	5689
0.364	5991
0.318	8942
0.273	14232
0.227	33048
0.182	34697
0.136	79209
0.091	98479

TABLE A-9

Breaking Time Distribution - AlRH100-3
Specimens Annelaed for One Hour
Conditioned at 100% R.H.

∇_{max} = 9849 psi
Zero time breaks = 6

$P(t_B)$	t_B (Seconds)
0.696	35
0.652	49
0.609	91
0.565	102
0.522	104
0.478	152
0.435	217
0.391	265
0.348	268
0.304	269
0.261	304
0.217	555
0.174	790
0.130	1157
0.087	1348
0.043	3513

TABLE A-10

Breaking Time Distribution -A24RH55
Specimens Annealed for 24 Hours
Conditioned at 55% R.H.

∇_{max} = 13566 psi

Zero time breaks = 4

$P(t_B)$	t_B (Seconds)	$P(t_B)$	t_B (Seconds)
0.881	81	0.381	3979
0.857	88	0.357	4784
0.833	93	0.333	5479
0.810	102	0.310	5619
0.786	201	0.286	8145
0.762	244	0.262	8907
0.738	247	0.238	9877
0.714	618	0.214	13383
0.690	641	0.190	13505
0.667	707	0.617	19414
0.643	737	0.143	21308
0.619	885	0.119	21482
0.595	909	0.095	21948
0.571	1041	0.071	42792
0.548	1220	0.048	49533
0.524	1385	0.024	92176
0.500	1995		
0.476	2581		
0.452	2801		
0.429	3042		
0.405	3709		

TABLE A-11

Breaking Time Distribution - LNP
Injection Molded Specimens Annealed for 24 Hrs.
Conditioned at 55% R.H.

$P(t_B)$	t_B (Seconds)
0.952	301
0.905	305
0.857	334
0.810	334
0.762	416
0.714	435
0.667	476
0.619	484
0.571	567
0.524	677
0.476	700
0.428	709
0.381	716
0.333	968
0.286	1799
0.238	2837
0.190	2970
0.143	3393
0.095	3755
0.048	6832

TABLE A-12

Data for Crack Propagation Rate Plots

Al RH 100

		$K_{max}(1-R)^{0.6}$	$\ln(\Delta a/\Delta t)$
154-2	1	5.90	-6.78
	2	5.91	-5.99
	3	5.92	-4.95
	4	5.94	-4.42
154-3	5	6.03	-6.91
	6	6.05	-5.96
	7	6.08	-2.65
	8	6.22	-2.53
	9	6.25	-1.63
	10	6.27	0.6418
154-5	11	5.87	-5.86
	12	5.90	-6.78
	13	5.94	-5.46
	14	6.04	-2.93
	15	6.07	-1.00
	16	6.23	1.97
	17	5.85	-5.28
154-1	18	5.96	-5.37
	19	6.00	-5.20
	20	5.99	-3.91
	21	6.08	-4.14
	22	6.11	-2.81
138	24	6.12	-4.72
	25	6.14	-3.17
	26	6.19	-2.00
	27	6.22	-1.44
	28	6.25	0.06

TABLE A-13

Data for Crack Propagation Rate Plots

Al RH 55

		$K_{max}(1-R)^{0.1}$	$\ln(\Delta a/\Delta t)$
O 156-3	1	6.11	-6.66
	2	6.20	-6.03
	3	6.26	-5.60
	4	6.29	-3.04
	5	6.31	-1.65
156-4	6	6.24	-4.42
	7	6.25	-3.65
	8	6.31	-5.08
	9	6.33	-3.25
	10	6.37	-2.51
	11	6.38	-1.76
	12	6.45	-0.413
156-2	13	6.07	-6.68
	14	6.16	-6.52
	15	6.21	-3.64
	16	6.25	-4.61
156-5	17	6.06	-5.90
	18	6.14	-6.80
	19	6.20	-5.77
	20	6.23	-5.78
	21	6.26	-4.54
	22	6.27	-2.19

TABLE A-14

Data for Crack Propagation Rate Plots

A 24 RH 55

		$K_{max}(1-R)^{0.4}$	ln ($\Delta a/\Delta t$)
126	1	6.42	-6.30
	2	6.45	-5.91
	3	6.48	-6.00
	4	6.5	-4.73
	5	6.52	-4.46
	6	6.55	-2.37
127	7	6.40	-6.84
	8	6.42	-5.93
	9	6.46	-5.24
	10	6.49	-4.49
	11	6.51	-3.79
	12	6.54	-3.35
	13	6.57	-1.43
129	14	6.53	-5.01
	15	6.54	-4.14
	16	6.55	-3.10
	17	6.59	-3.56
	18	6.63	-3.12
	19	6.66	-1.55
	20	6.71	-1.07
	21	6.76	0.11
144	22	6.37	-8.14
	23	6.38	-6.03
	24	6.46	-5.99
	25	4.48	-4.79
	26	6.51	-5.76
	27	6.54	-5.17
	28	6.55	-3.63
	29	6.56	-2.34

TABLE A-15

Apparent Fracture Toughness Obtained at
Different R Values During Crack Propagation Experiments

Sample	Experiment	K_{app}	R
A24RH 55	127	912.2	0.42
	129	988.2	0.18
	143	1077.6	0.43
	144	1263.2	0.73
AIRH 55	156-2	576.2	0.2
	156-3	602.2	0.4
	156-4	670.0	0.11
	156-5	606.8	0.5
AIRH 100	141	634.4	0.14
	154-2	561.4	0.21
	154-3	627.1	0.16
	154-5	575.8	0.18

TABLE A-16

Threshold Values Observed During
Crack Propagation Rate Experiments

Population	Experiment	K_{max}	R	ln ERD	ln V
A1RH100	154-2	493.9	0.419	5.58	-6.07
	154-3	440.8	0.146	6.10	-6.22
A1RH55	156-5	429.8	0.412	6.01	-6.65
A24RH55	126	793.6	0.52	6.38	-6.91
	144	1018.2	0.714	6.43	-8.11
	143	915.1	0.429	6.59	-9.21

Table A-17

Data for $\sigma_B(L_i)$ vs $t_B(L_i)$ Curve

A 1/2 RH55

P	log t_B	log σ_B
0.1	4.176	4.158
0.2	3.929	4.140
0.3	3.724	4.127
0.4	3.580	4.114
0.5	3.342	4.102
0.6	3.114	4.088
0.7	2.748	4.074
0.8	2.255	4.055

AlRH100

P	log σ_B	log t_{B-1}	log t_{B-2}	log t_{B-3}
0.05	4.104			3.230
0.1	4.092		4.643	3.079
0.2	4.076	4.869	4.260	2.845
0.3	4.064	4.301	4.0	2.653
0.4	4.057	3.964	3.732	2.447
0.5	4.045	3.653	3.477	2.190
0.6	4.033	3.362	3.161	1.833
0.7	4.021	2.954	2.799	
0.8	4.003	2.477	2.362	
0.9	3.973	1.778	1.531	

TABLE A-18

Shifted Data for $t_B(L_i)$ vs $\sigma_B(L_i)$ Master Curve

		$\log (t_B)_s$		$\log (t_B)_c$
P	$\log \sigma_B$	AIRH100-1	AIRH100-3	AIRH100-2
0.1	4.092		4.233	4.643
0.2	4.076	4.332	3.904	4.260
0.3	4.064	3.797	3.647	4.0
0.4	4.057	3.494	3.375	3.732
0.5	4.045	3.215	3.054	3.477
0.6	4.033	2.964	2.618	3.161
0.7	4.021	2.601		2.799
0.8	4.003	2.179		2.362
0.9	3.973	1.585		1.531

TABLE A-19

Generation of a Single Fatigue Distribution Curve (Fig. 29) by the Use of Crack Propagation Law and Breaking Strength Distribution

Starting Point: $\sigma_{max} = 11250$ at ERD = ERD crit. = 635
$P(\sigma_{max}) = 0.815$

	P	max PSI	ERD	$\dot{a}\frac{cm}{min}$	t_B (sec)
	0.1	14,400	496.1	3.14×10^{-3}	8.2×10^{3}
	0.2	13,800	517.7	4.73×10^{-3}	5.4×10^{3}
	0.3	13,400	533.1	6.36×10^{-3}	4.05×10^{3}
	0.4	13,030	548.3	8.62×10^{-3}	3.0×10^{3}
Reference:	0.5	12,650	564.7	1.227×10^{-2}	2.1×10^{3}
	0.6	12,290	581.3	1.84×10^{-2}	1.4×10^{3}
	0.7	11,860	602.3	3.55×10^{-2}	7.26×10^{2}

Table B-1

FATIGUE CRACK PROPAGATION RATE DATA FOR

GRAPHITE REINFORCED NYLON (@ 55 PERCENT HUMIDITY)

a in.	Pmean lb.	ΔP lb.	Pmax. lb.	Kmax. x 10^3	ΔK x 10^3	da/dt x 10^{-4} in/min.
0.5078	45.0	12.5	57.5	5.132397	2.231477	7.827752
0.5078	50.0	5.0	55.0	4.909249	0.8925908	1.083011
0.5078	50.0	7.5	57.5	5.132397	1.338886	4.806815
0.6178	40.0	7.5	47.5	4.705326	1.485892	4.641100
0.6178	45.0	10.0	55.0	5.998272	1.981190	14.86364
0.6178	45.0	12.5	57.5	5.695921	2.476487	57.54656
0.6178	50.0	7.5	57.5	5.695921	8.485892	21.57997
0.6178	50.0	10.0	60.0	5.94357	1.981190	96.99166
0.6178	50.0	12.5	62.5	6.191218	2.467487	370.6001
0.7178	40.0	10.0	50.0	5.373430	2.149372	23.53524
0.7178	40.0	12.5	52.5	5.642102	2.686715	112.4482
0.7178	45.0	7.5	52.5	5.642102	1.612029	27.05472
0.7178	45.0	1.0	55.0	5.910773	2.149372	134.9354

FATIGUE CRACK PROPAGATION RATE DATA FOR GRAPHITE REINFORCED NYLON (@ 55 PERCENT HUMIDITY (Cont.)

a in.	Pmean lb.	ΔP lb.	Pmax. lb.	Kmax. x 10^3	ΔK x 10^3	da/dt x 10^{-4} in./min.
0.7178	45.0	11.5	56.5	6.071976	2.471778	265.3597
0.7178	45.0	12.5	57.5	6.179445	2.68715	1207.862
0.7178	50.0	5.0	55.0	5.910773	1.074686	34.20014

Table B-2

FATIGUE CRACK PROPAGATION RATE DATA FOR

KEVLAR REINFORCED NYLON (@ 55 PERCENT HUMIDITY)

a in.	Pmean lb.	ΔP lb.	Pmax. lb.	Kmax. x 10^3	ΔK x 10^3	da/dt x 10^{-4} in/min.
0.500	40.0	5.0	45.0	5.631122	1.251361	4.326551
0.500	40.0	7.5	47.5	5.943962	1.877041	7.617170
0.500	45.0	5.0	50.0	6.256803	1.251361	7.115964
0.500	45.0	7.5	52.5	6.569643	1.877041	13.10082
0.500	45.0	12.5	57.5	7.195323	3.128401	37.84354
0.500	45.0	15.0	60.0	7.569643	3.754082	109.8637
0.620	40.0	7.5	47.5	6.750189	2.131639	24.25972
0.620	40.0	10.0	50.0	7.105462	2.842185	21.82466
0.620	45.0	12.5	57.5	7.460735	3.552731	56.11743
0.620	45.0	5.0	50.0	7.105462	1.421092	13.25956
0.620	45.0	7.5	52.5	7.460735	2.131639	24.92245
0.620	45.0	10.0	55.0	7.816008	2.842185	35.15596
0.620	45.0	12.5	57.5	8.171281	3.552731	53.15021

FATIGUE CRACK PROPAGATION RATE DATA FOR KEVLAR REINFORCED NYLON (@ 55 PERCENT HUMIDITY)(Cont.)

a in.	Pmean lb.	ΔP lb.	Pmax. lb.	Kmax. x 10^3	ΔK x 10^3	da/dt x 10^{-4} in./min.
0.765	40.0	5.0	45.0	11.16865	2.481921	32.47872
0.765	40.0	7.5	47.5	11.78913	3.722882	64.51138
0.765	40.0	10.0	50.0	12.40961	4.963803	95.03371
0.765	40.0	12.5	52.5	13.03009	6.204803	201.1229

Table B-3

FATIGUE CRACK PROPAGATION RATE DATA FOR

PRD/GRAPHITE REINFORCED NYLON (@ 100 PERCENT HUMIDITY)

a in.	Pmean lb.	ΔP lb.	Pmax. lb.	Kmax. x 10^4	ΔK x 10^3	da/dt x 10^{-4} in./min.
0.660	35.0	10.0	45.0	1.100878	4.892789	0.9103563
0.660	35.0	15.0	50.0	1.223197	7.339184	1.198417
0.660	40.0	12.5	52.5	1.284357	6.115987	1.134633
0.660	40.0	15.0	55.0	1.345517	7.339184	1.304055
0.765	35.0	10.0	45.0	1.681452	7.473120	1.628108
0.765	30.0	15.0	45.0	2.055108	11.20968	2.651147
0.765	35.0	20.0	55.0	1.82559	14.94624	6.259829
0.805	35.0	10.0	45.0	1.82559	8.113735	2.333332
0.805	35.0	15.0	45.0	1.825590	12.17060	5.015576
0.805	42.5	10.0	52.5	2.125855	8.113735	3.186184
0.806	35.0	10.0	45.0	1.941786	8.630162	4.419081
0.860	30.0	15.0	45.0	1.941786	12.945524	11.97934
0.860	40.0	12.5	52.5	2.265418	10.7877	62.27913
0.860	40.0	15.0	55.0	2.373295	12.945524	15.31301

FATIGUE CRACK PROPAGATION RATE DATA FOR HYBRID LAMINA REINFORCED NYLON (@ 100 PERCENT HUMIDITY) (Cont.)

a in.	Pmean lb.	ΔP lb.	Pmax. lb.	K max. x 10^4	ΔK x 10^3	da/dt x 10^{-4} in./min.
0.860	45.0	12.5	57.5	2.481172	10.78770	8.294053
0.985	35.0	10.0	45.0	1.670494	7.424419	15.45071
0.985	35.0	15.0	50.0	1.856105	11.13663	6.65750
0.985	37.5	17.5	55.0	2.041715	12.99273	4.349622
1.045	35.0	10.0	45.0	0.911205	4.049803	0.411386
1.045	35.0	15.0	50.0	1.012451	6.074705	1.037092
1.045	45.0	7.5	52.5	1.063073	3.037352	0.3761494
1.045	40.0	12.5	52.5	1.063073	5.062254	0.9246066
1.045	45.0	15.0	60.0	1.214941	6.074705	1.100906

Table B-4

FATIGUE CRACK PROPAGATION RATE DATA FOR

PRD/GRAPHITE REINFORCED NYLON (@ 55 PERCENT HUMIDITY)

a in.	Pmean lb.	ΔP lb.	Pmax. lb.	K max. x 10^3	ΔK x 10^3	da/dt x 10^{-4} in./min.
0.620	40.0	7.5	47.5	5.497405	1.736023	1.365601
0.620	40.0	12.5	52.5	6.076079	2.893371	27.52839
0.620	45.0	7.5	52.5	6.076079	1.736023	17.25514
0.695	40.0	5.0	45.0	5.141612	1.142580	3.824867
0.695	40.0	10.0	50.0	5.712902	2.285161	18.59532
0.695	40.0	12.5	52.5	5.998547	2.856451	22.32713
0.695	45.0	5.0	50.0	5.712902	1.14258	6.503796
0.695	45.0	12.5	57.5	6.569838	2.856451	27.38847
0.695	45.0	15.0	60.0	6.855483	3.427741	85.14778
0.805	40.0	5.0	45.0	5.118415	1.137425	3.715170
0.805	40.0	7.5	47.5	5.402771	1.706138	10.42278
0.805	40.0	10.0	50.0	5.687127	2.274851	20.76946
0.805	45.0	5.0	50.0	5.687127	1.137425	5.649100
0.805	45.0	12.5	57.5	6.540197	2.843564	24.81449
0.805	50.0	7.5	57.5	6.540197	1.706138	13.54965
0.805	50.0	10.0	60.0	6.824553	2.274851	55.40770

FATIGUE CRACK PROPAGATION RATE DATA FOR

HYBRID LAMINA REINFORCED NYLON (@ 55 PERCENT HUMIDITY)(Cont.)

a in.	Pmean lb.	ΔP lb.	Pmax. lb.	Kmax. x 10^3	ΔK x 10^3	da/dt x 10^{-4} in./min.
0.830	37.5	7.5	45.0	5.175602	1.725201	7.693703
0.830	35.0	10.0	45.0	5.175602	2.300268	11.21808
0.830	32.5	12.5	45.0	5.175602	2.875334	13.712614
0.830	30.0	15.0	45.0	5.175602	3.450401	17.75534
0.830	35.0	15.0	50.0	5.750669	3.450401	30.16776
0.830	37.5	12.5	50.0	5.750669	2.875334	25.25223
0.830	40.0	10.0	50.0	5.750669	2.300268	18.45115
0.830	47.5	7.5	55.0	6.325736	1.725201	22.04860
0.830	45.0	10.0	55.0	6.325736	2.300268	28.22816
0.830	42.5	12.5	55.0	6.325736	2.875334	32.69513
0.830	40.0	15.0	55.0	6.325736	3.450401	45.50694
0.880	25.0	15.0	40.0	4.808030	3.505022	13.23278
0.880	27.5	12.5	40.0	4.808030	3.005019	9.877467
0.880	30.0	10.0	40.0	4.808030	2.404015	8.933261
0.880	37.5	7.5	40.0	4.808030	1.803011	5.813103

FATIGUE CRACK PROPAGATION RATE DATA FOR

HYBRID LAMINA REINFORCED NYLON (@ 55 PERCENT HUMIDITY) (Cont.)

a in.	Pmean lb.	ΔP lb.	Pmax. lb.	Kmax. x 10^3	ΔK x 10^3	da/dt x 10^{-4} in./min.
0.880	35.0	10.0	45.0	5.409033	2.404015	18.23515
0.880	35.0	15.0	50.0	6.010037	3.606022	42.53194
0.880	37.5	12.5	50.0	6.010037	3.005019	32.32445
0.880	40.0	10.0	50.0	6.010037	2.404015	25.16881
0.880	42.5	7.5	50.0	6.010037	1.803011	18.01767
0.880	45.0	10.0	55.0	6.611041	2.404015	56.57964
0.880	42.5	12.5	55.0	6.611041	3.005019	62.88687
0.880	40.0	15.0	55.0	6.611041	3.606022	78.32395
0.940	25.0	15.0	40.0	5.283138	3.962353	25.40990
0.940	27.5	12.5	40.0	5.283138	3.301961	20.93623
0.940	30.0	10.0	40.0	5.283138	2.641569	17.11353
0.940	22.5	7.5	40.0	5.283138	1.981177	12.47416
0.940	37.5	7.5	45.0	5.943530	1.981177	17.98560
0.940	35.0	10.0	45.0	5.943530	2.641569	25.20859
0.940	32.5	12.5	45.0	5.943530	3.301061	32.16501

FATIGUE CRACK PROPAGATION RATE DATA FOR

HYBRID LAMINA REINFORCED NYLON (@ 55 PERCENT HUMDITY) (Cont.)

a in.	Pmean lb.	ΔP lb.	Pmax. lb.	Kmax. x 10^3	ΔK x 10^3	da/dt x 10^{-4} in./min.
0.940	30.0	15.0	45.0	5.943530	3.962353	40.00000
0.940	35.0	15.0	50.0	6.603922	3.962353	93.57825
0.940	37.5	12.5	50.0	6.603922	3.301961	76.48370
0.940	40.0	10.0	50.0	6.603922	2.641569	62.15769
0.940	42.5	7.5	50.0	6.603922	1.981177	30.57303
0.940	47.5	7.5	55.0	7.264315	1.981177	7.150401
0.940	45.0	10.0	55.0	7.264315	2.641569	109.6140
0.940	40.0	15.0	55.0	7.264315	3.962353	221.7030
0.940	42.5	12.5	55.0	7.264315	3.301961	165.7822

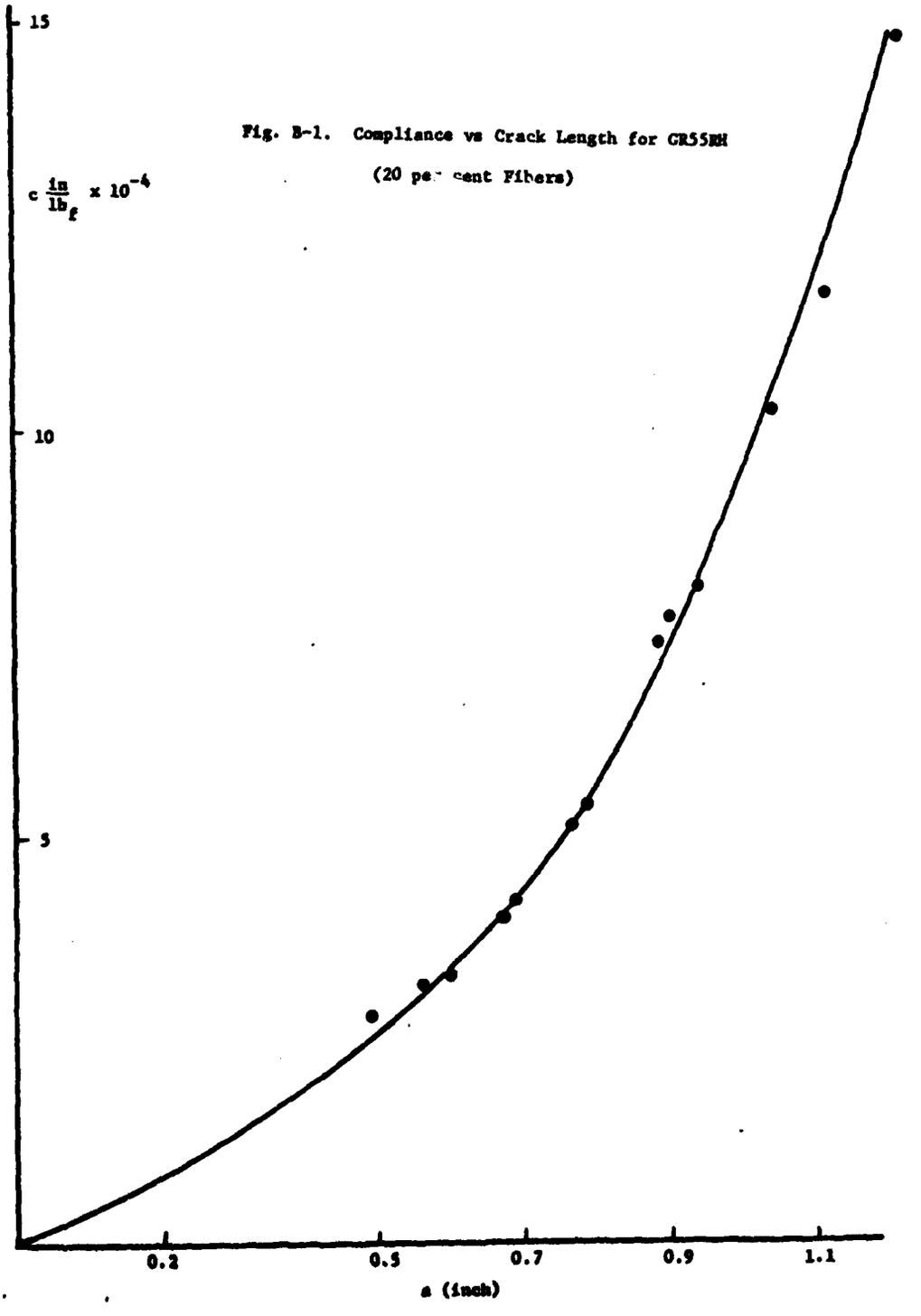

Fig. B-1. Compliance vs Crack Length for GR55BH (20 per cent Fibers)

Fig. B-2. Compliance vs Crack Length for PR55RH

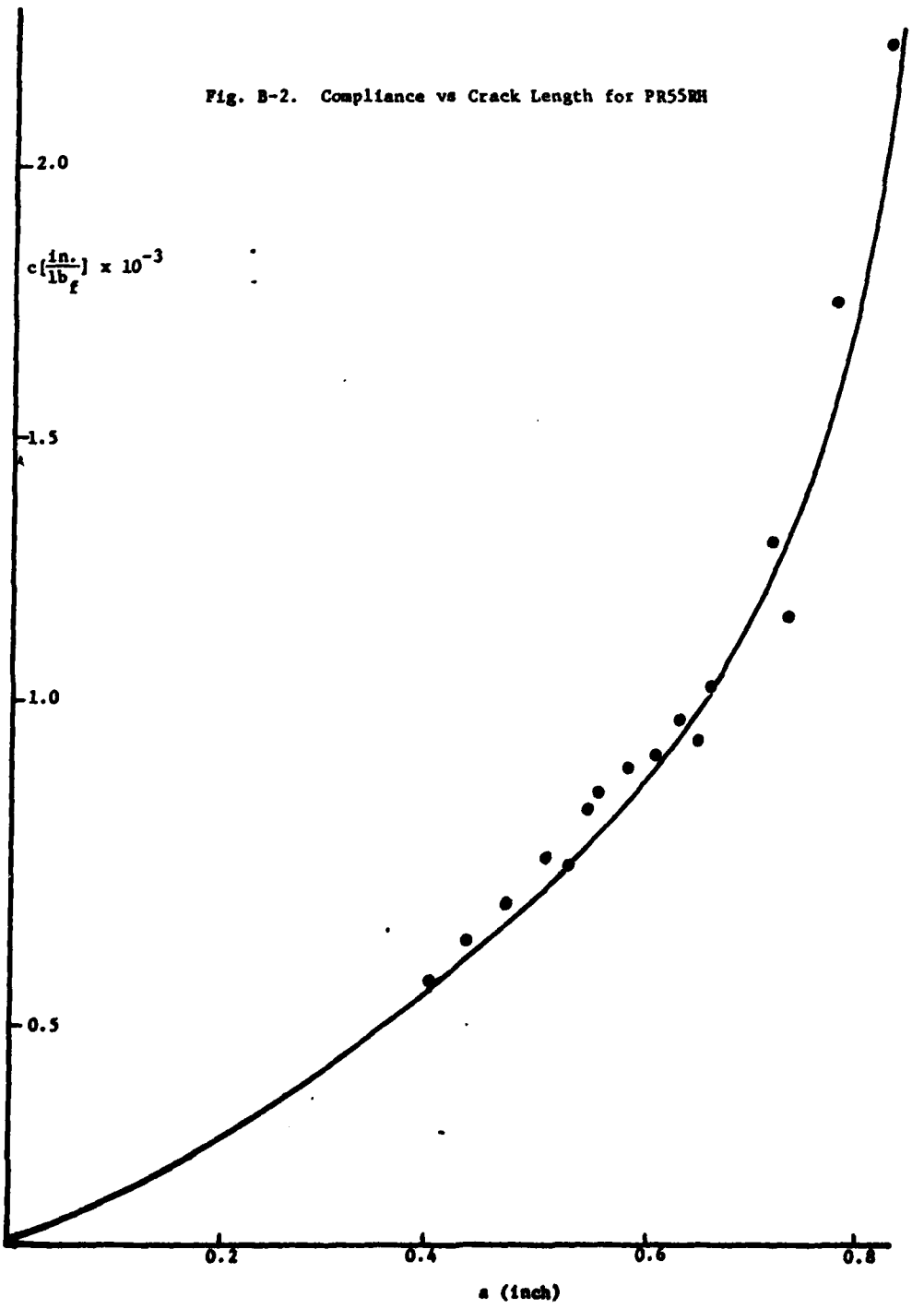

Fig. B-3. Compliance vs Crack Length for HYL55RH

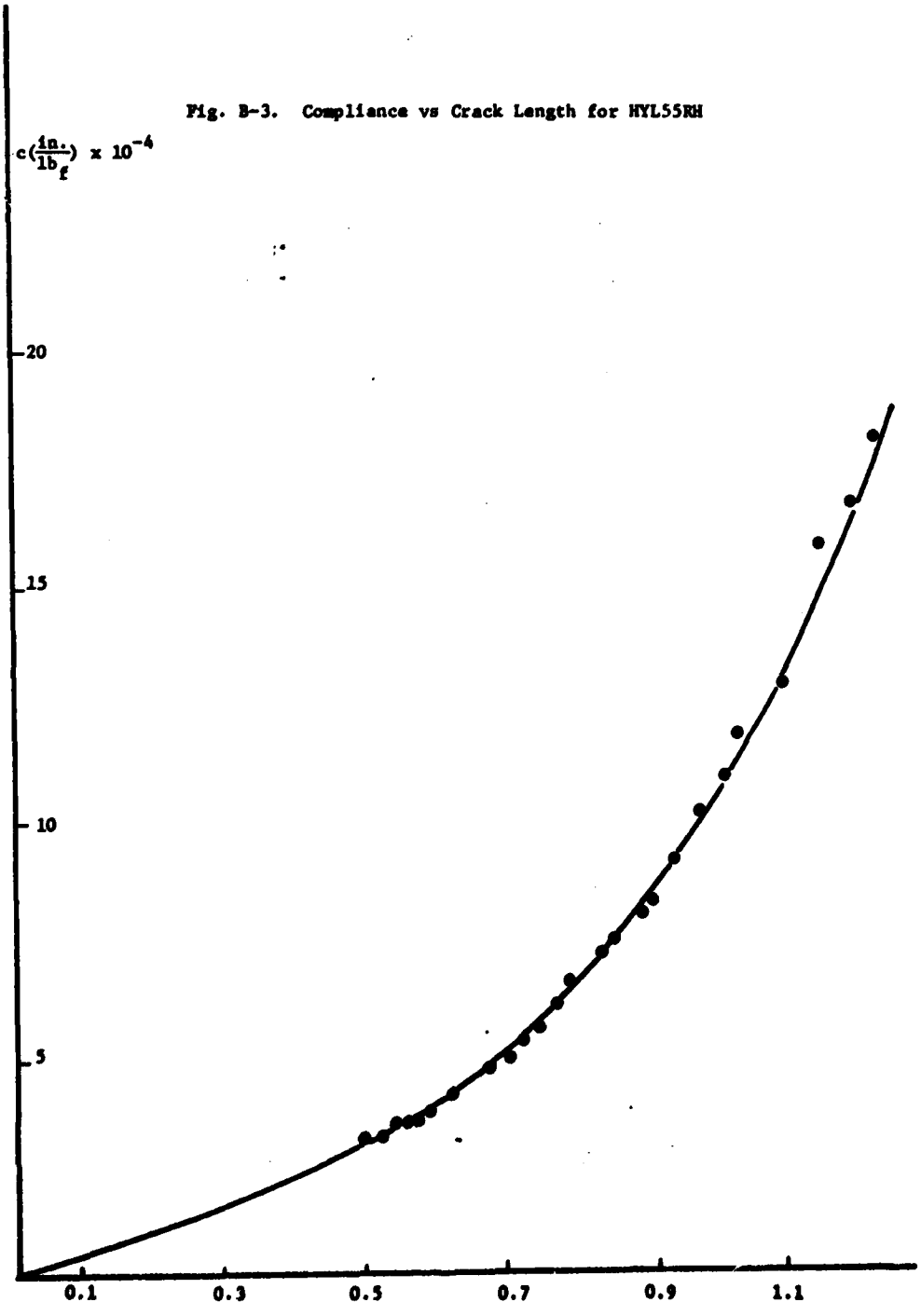

Fig. B-4. Compliance vs Crack Length for HYL100RH

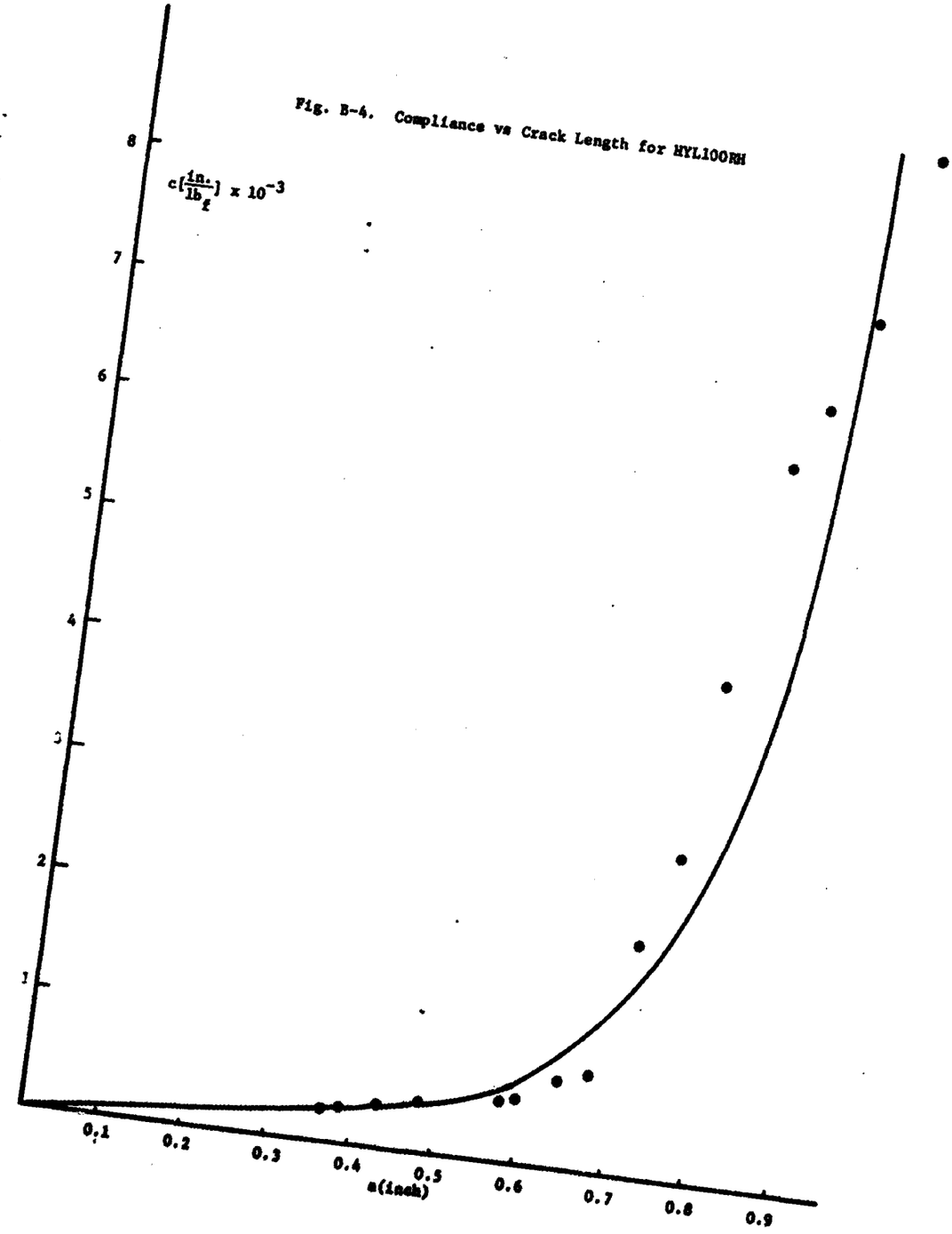

Army Materials and Mechanics Research Center,

Watertown, Massachusetts 02172
A STUDY OF THE FATIGUE BEHAVIOR OF FIBER REINFORCED COMPOSITES
A. T. DiBenedetto, G. Salee
University of Connecticut, Storrs, CT 06268

Technical Report AMMRC CTR 77-12, March, 1977
103 pp illustrations - tables, Contract DAAG46-75-C-0064, D/A Project 1T162105AH84
AMCMS Code 612105H80411, Final Report,
March 1, 1975 to June 30, 1976

AD_____

UNCLASSIFIED
Unlimited Distribution

Key Words
Fatigue (Materials)
Fiber Composites
Graphite Fibers
Polyaramid Fibers

The objects of this study were to develop a statistical model for characterizing the reliability of short fiber reinforced plastics and to develop an experimental method for measuring crack propagation rates in fiber reinforced plastics. The fatigue behavior of graphite and polyaramid fiber reinforced nylon is reported.

Army Materials and Mechanics Research Center,

Watertown, Massachusetts 02172
A STUDY OF THE FATIGUE BEHAVIOR OF FIBER REINFORCED COMPOSITES
A. T. DiBenedetto, G. Salee
University of Connecticut, Storrs, CT 06268

Technical Report AMMRC CTR 77-12, March, 1977
103 pp illustrations - tables, Contract DAAG46-75-C-0064, D/A Project 1T162105AH84
AMCMS Code 612105H80411, Final Report,
March 1, 1975 to June 30, 1976

AD_____ _____

UNCLASSIFIED
Unlimited Distribution

Key Words
Fatigue (Materials)
Fiber Composites
Graphite Fibers
Polyaramid Fibers

The objects of this study were to develop a statistical model for characterizing the reliability of short fiber reinforced plastics and to develop an experimental method for measuring crack propagation rates in fiber reinforced plastics. The fatigue behavior of graphite and polyaramid fiber reinforced nylon is reported.

Army Materials and Mechanics Research Center,

Watertown, Massachusetts 02172
A STUDY OF THE FATIGUE BEHAVIOR OF FIBER REINFORCED COMPOSITES
A. T. DiBenedetto, G. Salee
University of Connecticut, Storrs, CT 06268

Technical Report AMMRC CTR 77-12, March, 1977
103 pp illustrations - tables, Contract DAAG46-75-C-0064, D/A Project 1T162105AH84
AMCMS Code 612105H80411, Final Report,
March 1, 1975 to June 30, 1976

AD_____

UNCLASSIFIED
Unlimited Distribution

Key Words
Fatigue (Materials)
Fiber Composites
Graphite Fibers
Polyaramid Fibers

The objects of this study were to develop a statistical model for characterizing the reliability of short fiber reinforced plastics and to develop an experimental method for measuring crack propagation rates in fiber reinforced plastics. The fatigue behavior of graphite and polyaramid fiber reinforced nylon is reported.

Army Materials and Mechanics Research Center,

Watertown, Massachusetts 02172
A STUDY OF THE FATIGUE BEHAVIOR OF FIBER REINFORCED COMPOSITES
A. T. DiBenedetto, G. Salee
University of Connecticut, Storrs, CT 06268

Technical Report AMMRC CTR 77-12, March, 1977
103 pp illustrations - tables, Contract DAAG46-75-C-0064, D/A Project 1T162105AH84
AMCMS Code 612105H80411, Final Report,
March 1, 1975 to June 30, 1976

AD_____ _____ _____

UNCLASSIFIED
Unlimited Distribution

Key Words
Fatigue (Materials)
Fiber Composites
Graphite Fibers
Polyaramid Fibers

The objects of this study were to develop a statistical model for characterizing the reliability of short fiber reinforced plastics and to develop an experimental method for measuring crack propagation rates in fiber reinforced plastics. The fatigue behavior of graphite and polyaramid fiber reinforced nylon is reported.